IAOS

International Association for Obsidian Studies

Bulletin

ISSN: 2310-5097

Number 59 **Summer 2018**

CONTENTS

NEWS AND INFORMATION

NEWS AND NOTES

Have news or announcements to share? Send them to IAOS.Editor@gmail.com for the next issue of the *IAOS Bulletin.*

CONSIDER PUBLISHING IN THE IAOS *BULLETIN*

The *Bulletin* is a twice-yearly publication that reaches a wide audience in the obsidian community. Please review your research notes and consider submitting an article, research update, news, or lab report for publication in the *IAOS Bulletin*. Articles and inquiries can be sent to IAOS.Editor@gmail.com Thank you for your help and support!

CALL FOR NOMINATIONS

Kyle Freund has just begun his responsibilities as IAOS President, and Rob Tykot has stepped into the position of Past President for the coming year. That means that it's now time for nominations for our next IAOS President. Elections will be held this winter and the winner announced at the 2019 IAOS meeting at the SAAs in Albuquerque. The winner will then serve as President-Elect for one year and begin the term of President in 2020. If you, or someone you know, would be interested in serving as IAOS President, please send a nomination to Kyle Freund at kylepfreund@gmail.com.

NOTES FROM THE PRESIDENT

As I begin my term, I want to thank the outgoing President Rob Tykot for his service. Rob has been a long-time member of IAOS and will no doubt continue to contribute to its growth and success.

For those of you who were unable to make it to the SAAs in Washington D.C. this April, you not only missed the IAOS business meeting but also the cherry blossoms blooming throughout the city. It was truly beautiful, and if you haven't been to D.C. in the spring I encourage you to do so.

IAOS is planning several initiatives in the upcoming year, and we look forward to your participation. The SAAs in 2019 will be in Albuquerque, and our Newsletter Editor, Carolyn Dillian, will be helping to organize a sponsored session in honor of Steve Shackley, a former IAOS President whose 30-plus-year career has spanned the fields of anthropology, archaeology, geology, and museum studies. The honor is well deserved, and I think I speak on behalf of everyone in saying that we look forward to seeing him.

There are a number of obsidian sources outside of Albuquerque, so IAOS is also looking into organizing a trip to visit one of them. Also on the horizon in May 2019 is the 2nd International Obsidian Conference in Budapest, Hungary, building upon the successful 2016 symposium on the island of Lipari, Italy. We will keep everyone posted!

On a personal note, I was fortunate enough to receive a grant for equipment and supplies in the newly-founded IRSC Archaeology and Paleosciences (APS) Laboratory, which will hopefully become a center for future obsidian studies.

Summer is here and like many of you, I'm also kicking off my field season, which will begin in Mérida, Mexico for the International Symposium on Archaeometry (ISA). Later, I will be in southeast Italy conducting subsurface coring at known prehistoric sites for datable materials; this work will hopefully identify areas for further excavation. I will end my summer in Sardinia where I will be analyzing a collection of prehistoric obsidian artifacts. As always though, I am feverishly trying to write up analyses I have already completed. Sigh…

Have a great summer!

Kyle Freund, IAOS President
Department of Anthropology
Indian River State College
kfreund@irsc.edu

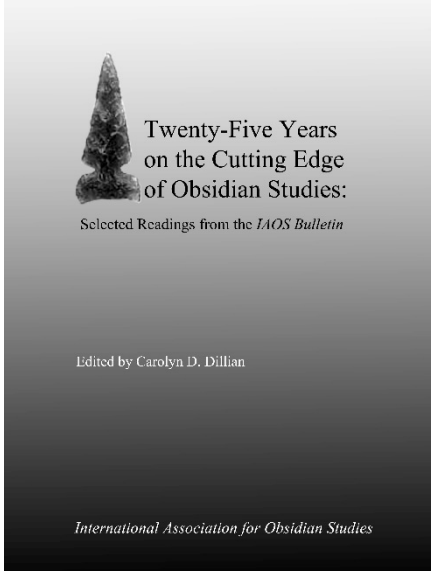

Twenty-Five Years on the Cutting Edge of Obsidian Studies: Selected Readings from the IAOS Bulletin

Edited volume available for purchase online!

As part of our celebration of the 25th anniversary of the IAOS, we published an edited volume highlighting important contributions from the *IAOS Bulletin.* Articles were selected that trace the history of the IAOS, present new or innovative methods of analysis, and cover a range of geographic areas and topics. The volume is now available for sale on the IAOS website for $10 (plus $4 shipping to U.S. addresses).

http://members.peak.org/~obsidian/iaos_publications.html

International addresses, please contact us directly at IAOS.Editor@gmail.com for shipping information.

Obsidian Sessions & Events for the 2019 SAA Meeting in Albuquerque, New Mexico, USA

We are beginning preliminary planning for the 2019 SAA meeting in Albuquerque, New Mexico, USA, which is scheduled for April 10-14, 2019. Information on the conference is here: http://www.saa.org/AbouttheSociety/AnnualMeeting/tabid/138/Default.aspx

We anticipate that this SAA meeting will be popular for obsidian researchers and the IAOS is prepared to host a variety of events, including our annual business meeting (see the SAA conference program for date, time, and location). We are currently in discussions for possible IAOS field trips, sponsored conference sessions, and a table in the SAA exhibit hall. We have also received early news that M. Steven Shackley will be receiving the Fryxell Award for 2019, so there will be a sponsored session honoring him and his work.

If you would like to participate in a session honoring Steve Shackley, please email Carolyn Dillian at cdillian@coastal.edu.

Please watch your email and the IAOS webpage for additional announcements about IAOS events, meetings, and trips in Albuquerque. If you are willing to assist with the IAOS table in the exhibit hall, please contact Kyle Freund at kfreund@irsc.edu

2nd Circular IOC 2019

Event

The International Obsidian Conference 2019 is a direct continuation of the 2016 Lipari Meeting (http://rtykot.myweb.usf.edu/Obsidian%202016/index.html). It is planning to deal with all aspects of obsidian studies, from geology to anthropology and instrumental analyses.

The planned sessions of the Conference are:

- Formation and geology of obsidian
- Obsidian sources and their characterisation
- Analytical / methodological aspects of obsidian studies
- Archaeological obsidian by chronological periods
- Lithic technology and use wear
- Obsidian hydration dating
- Dating of geological obsidian
- Exploring the allure of obsidian: symbolic, social, and practical values for obsidian
- Super-long distance movement of obsidian in prehistory: why, how, and what for?

You will find all necessary information on our conference and registration webpage:
http://ioc-2019.ace.hu
We would ask you to check the webpage from time to time for any updated information.

Venue

The Conference has two venues, i.e. the main building of the
Hungarian National Museum in Budapest, Hungary
and the **Rákóczi Museum** at Sárospatak
This means that the Conference will have a tight schedule. We will try to make all we can to facilitate your participation by organising Conference buses and help in booking accommodation in Sárospatak.

Registration

Registration will be implemented via the Conference web page (http://ioc-2019.ace.hu/) starting from May 2018.

Deadline for registration: 1 April 2019

Registration fee:
full registration fee 100 EUR
distance participants 50 EUR
early bird registration (until 15 January 2019) 80 EUR
students and accompanying persons 50 EUR
early bird registration (until 15 January 2019) 40 EUR

'Early bird registration' is accepted with payment prior to 15 January: this option is not available for distance participants.

Payment

Payment will be realised via bank transfer.
Registration and other conference related costs should be transferred to the account of the Hungarian National Museum (1088 Budapest, Múzeum krt. 14-16.) curated at the Hungarian State Treasury (Magyar Államkincstár):

account number: 10004885-10002010-01016431
IBAN number: HU03 1000 4885 1000 2010 0101 6431„account with institution": Hungarian State Treasury (Magyar Államkincstár)

SWIFT code: HUSTHUHB„correspondent": Hungarian National Bank (Magyar Nemzeti Bank)

SWIFT code: MANEHUHB

preferentially at the same time as the registration but not later than 30 April 2019.

Communications

The official language of the conference is English.
Only one lecture for each (registered) participant can be accepted. Posters are expected without limit. Please indicate their number precisely on the Registration Form.
As the conference time is limited, organisers may have to limit the number of oral presentations.

Abstract submission:
For abstract submission please use our webpage (see Registration). Please prepare 3 – 5 keywords. The abstract should not be longer than 300 words. The abstract can only be accepted when at least one of the authors is registered. Please contact us if you encounter any problem. The deadline for abstract submission is **1 April 2019.**

Proceedings: We are planning to publish the Proceedings of the Conference hopefully in one volume. Decision on the means and place will be made later on. Please check our webpage for details

Program: We aim to create the program as fast as possible. The program will be published on the webpage and can be downloaded there.

The length of oral presentations is expected to be 20 minutes including discussion. Please prepare them in a common presentation format (ppt, pps).
Internet video conference possibility will be provided for registered participants but we definitely prefer your personal presence!

The poster sections will be held on the corridors of the Sárospatak Museum.
The posters should be planned as standing (portrait) orientation and their size must not exceed A0 (841 x 1189 mm).
You can send lectures / posters in advance if you like, for checking technically on our devices or printing: please specify your needs on the Registration form.

Excursions

On the second and third day excursions to Hungarian (Mád and Tolcsva) and Slovakian (Brehov and Viničky) obsidian sources will be organised as part of the Conference.
A post-conference tour to the so-called Carpathian 3 sources (around Rokosovo, Ukraine) is anticipated depending on possibilities at extra costs.

Please keep in your mind that for citizens of a number of countries visa is required to Ukraine.
Remember that you have to cross the EU (Schengen) border twice, that means multiple visa.
Please visit the Consular Service website of your respective countries for more information.

Satellite events

27 May 2019
In the Hungarian National Museum we are planning to open a temporary exhibition on obsidian entitled „**Beyond the Glass Mountains**" on various aspects of obsidian studies. The exhibition is designed in a way to suit the purposes of an itinerant exhibition we are planning to circulate in the neighbouring countries.

28 May 2019
In the Rákóczi Museum of the HNM we are planning a chamber exhibition on obsidian from the material of local collections of geological and archaeological obsidians under the title „**Our glass, our past**".
We are also planning to install conference posters on an open exhibition space where they will be temporarily available for the general public.

Social events

26 May 2019
The Conference will start with an Ice-Breaking Party at the Mineralogy Department of the Eötvös University, 1/C Pázmány Péter sétány Budapest, H-1117.
The Exhibition Hall of the Department is hosting the oldest mineralogical collection of Hungary, transported piece by piece to a modern building.
A small Archaeometry exhibition, used in teaching students of geosciences, is also part of the exhibition.

29 May 2019
Conference Dinner will be organised at Sárospatak, Vár Restaurant after the excursion to the Slovakian sources.

Accommodation

Budapest is a large city with all kinds of accommodation available. We kindly ask You to make your own arrangements, in time and on time. Please check the Conference events and venues and plan your travel and accommodation accordingly.
Sárospatak is a charming small town in the northeastern part of the country. The organisers will book hotel and hostel accommodation between 27 to 30 May to secure availability for conference and participants, therefore the booking of hotels and payment for Sárospatak will be arranged via the Hungarian National Museum (see Registration Form). We give the price for rooms, you may team for double rooms in Hotel Bodrog or houses in the Motel.

Transport

We are planning to provide free transport for registered conference participants by bus between the venues from Budapest to Sárospatak and back to facilitate travelling. The same bus(es) will be used for the conference excursions. Nevertheless, you may prefer to use your own solutions (please mark your choice on the Registration Form).
The standard conference bus transport will be implemented on the 27th May (after conference day in HNM) and back on the 30th May. The buses will reach Budapest early afternoon, for those who select the Miskolc visit, in the evening only. The excursion to the Ukrainian source (30 May 2019) has a special fee, transport back to Budapest is included (arrival late in the evening). Please calculate with this when you are planning your travel and accommodation: when in doubt, please feel free to contact us.

Parking

Parking in Budapest is difficult and expensive. You may inquire at the selected hotel for parking facilities.
For those of you arriving by car and taking advantage of the free conference transfer (Budapest-Sárospatak) we suggest to use the parking facilities of the Hungarian National Museum on a fee for the museum staff (250 HUF/day, around 1 US$ and a little less than 1 Euro). If you need this service, please fill out the Registration Form accordingly.

Weather

The weather in the end of May is typically nice and warm, with an average daily temperature of 15-17°C and 14 rainy days. Be prepared for rain and muddy soil, anyways.

Local Organising Committee

T. Biró, Katalin - HNM, Markó, András - HNM, Kasztovszky, Zsolt - MTA EK, Weiszburg, Tamás - ELU, Csengeri, Piroska - HOM, Kereskényi, Erika - HOM, Péterdi, Bálint - MFGI, Pap, Gábor - HNHM, Rajczy, Miklós - HNHM, Tamás, Edit - HNM-RM, Hegyi, Borbála - HNM-RM, Szepesi, János – VRG, Bačová, Zuzana & Bačo, Pavel SGI, Přichystal, Antonín MU, Rácz, Béla KMF, Ryzhov, Sergei, TSNU

International Scientific Committee

Ono, Akira - Meiji University, Tokyo, Japan, Glascock, Michael - University of Missouri, Columbia, MO, USA, Kuzmin, Yaroslav - Institute of Geology & Mineralogy, Siberian Branch of the Russian Academy of Sciences, Novosibirsk, Russia, Tykot, Robert - University of South Florida, Tampa, FL, USA, Andrea Vianello, Lipari, Italy / Tampa, Florida, Torrence, Robin - Australian Museum, Sydney, Australia, Le Bourdonnec, François-Xavier - Université Bordeaux Montaigne, Pessac, France, Lexa, Jaroslav - Earth Sciences Institute of the Slovak Academy of Sciences, Bratislava, Slovakia

Please forward this circular to anybody who might be interested.
Looking forward to see you in 2019!

Registration is expected to be online
should you meet difficulties contact the organisers by email personally:
ioc-2019@hnm.hu

A COMPUTER PROGRAM IN MatLab FOR OBSIDIAN HYDRATION AGE COMPUTATIONS

Alexander K. Rogers
Archaeology Curator, Maturango Museum

Abstract

This paper describes and documents a computer program, written in MatLab, for performing obsidian hydration age calculations efficiently. To avoid errors and make the calculation more exact, it computes effective hydration temperature (EHT) by numerical integration rather than by algebraic approximations. For further accuracy improvement, it computes the activation energy of the obsidian from the input hydration rate and uses this value in computing EHT, rather than using a nominal value. It accounts for artifact burial depth explicitly; since the length of time an artifact was buried is frequently unknown or difficult to assess, it computes ages based on surface conditions, depth conditions, and a mixed condition in which the artifact was buried at the recovery depth half its life and on the surface the other half. It accommodates large data sets by using comma-separated variable (.csv) files for input and output, and the output files are easily converted to .xls files for analysis. Source code has been uploaded to the IAOS website, and is available for free use by scholars. Working papers providing data for the code are also on the IAOS website. The code will execute in MatLab or in Gnu Octave, a freeware alternative.

Introduction

Doing a rigorous computation of archaeological ages based on obsidian hydration requires a significant effort in mathematics, especially the calculation of effective hydration temperature (EHT). Small jobs can be done with Microsoft Excel, although even there one must make approximations to make the process feasible, and the process is error-prone. To avoid the errors and make the calculation more exact, I have developed a computer program in MatLab to perform the dating calculations. To improve accuracy, it computes EHT by numerical integration rather than by algebraic approximations, which is impractical in MS Excel. For further accuracy improvement, it computes the activation energy of the obsidian from the input hydration rate and uses this value in computing EHT, rather than using a nominal value. It accounts for artifact burial depth explicitly; since the length of time an artifact was buried is frequently unknown or difficult to assess, it computes ages based on surface conditions, depth conditions, and a mixed condition in which the artifact was buried at the recovery depth half its life and on the surface the other half, so the analyst can choose which is most appropriate.

A key input to any obsidian hydration date (OHD) analysis is the site temperature regime, which is described by three parameters: annual average temperature, annual temperature variation (hot-month mean minus cold-month mean) and mean diurnal variation. These parameters must reflect long-term data (30 years is the meteorological standard, per Cole 1970). The code as it stands incorporates a temperature model for eastern California and the western Great Basin, in which the temperature parameters are computed from site elevation above mean sea level (amsl). A user working in another area could modify the model as needed.

The present code includes hydration rates for ten obsidian sources which are commonly encountered in eastern California. Again, a user can substitute obsidian data for other areas. The obsidian data required are a hydration rate in μ^2/1000 years at 20°C, and

an estimate of the coefficient of variation of the rate due to intra-source intrinsic water variation.

Finally, the code computes a best estimate of the age error standard deviation, based on five primary sources of uncertainty: hydration rim measurement; errors in the hydration rate ascribed to a source; intra-source rate variability due to uncontrolled intrinsic water in the obsidian; errors in reconstructing the temperature history; and errors caused by site formation processes.

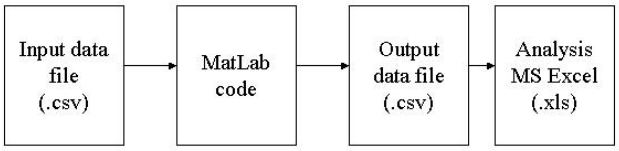

Figure 1. Overall work process for MatLab code in obsidian hydration dating

To facilitate big analytical jobs with many data points, input data are loaded by creating an MS Excel spreadsheet (.xls) and saving it as a comma-separated variable (.csv) file. The MatLab code reads this file (Figure 1) and computes ages and age accuracies. It then outputs to a file in .csv format, which is easily converted to .xls format for analysis. Figure 2 shows the structure of the MatLab code. The program will literally run hundreds of data points in a second or two, and saves a world of work and mistakes. The remainder of this paper documents the code in detail, including the references for the various data sources. A copy of the code is on the IAOS website, and is available for use by anyone who knows MatLab and has access to it. In addition, the working papers cited as data sources are uploaded so they are accessible, although papers subject to copyright restriction are not.

Hydration Physics

Obsidian is an alumino-silicate, or rhyolitic, glass, formed by rapid cooling of magma under the proper geologic conditions. Like any other glass, it is not a crystal, and thus it lacks the lattice structure typical of crystals at the atomic level, but it does possess a matrix-like structure exhibiting some degree of spatial order (Doremus 1994: 27, Fig. 2; 2002: 59-73). Obsidian is typically about 75% SiO_2 and about 20% Al_2O_3 by weight, the remainder being trace elements, some of which are source-specific (Doremus 2002: 109, Table 8.1; Hughes 1988; Stevenson et al. 1998; Zhang et al. 1997). The anhydrous composition, or chemical composition independent of water, of obsidian from a wide variety of sources has been shown to be remarkably consistent, within a few tenths of a weight percent (Zhang et al. 1997). The minute interstices within the glass matrix, on the order of 0.1 - 0.2 nanometer in diameter, are where water penetration takes place.

Obsidian also contains small amounts of natural water, known as intrinsic water or structural water, resulting from the magma formation process. The amount is generally <2% by weight in natural obsidian, although

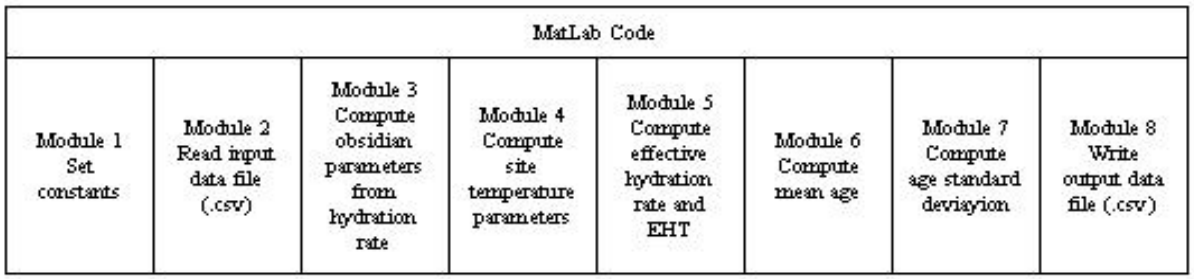

Figure 2. Module structure of the MatLab code.

cases of somewhat higher concentrations are occasionally encountered.

Hydration of obsidian is a diffusion-reaction process (Doremus 2002; Zhang 2008). "Diffusion" is, by definition, a mass transport process driven by a concentration gradient, while "reaction" is a process by which a fraction of the diffusing water reacts with the atoms of the glass matrix and becomes immobile. When an obsidian surface is exposed to the atmosphere, water molecules adsorb onto the surface. Subsequently a fraction of the adsorbed water is absorbed into the glass, in a process by which a water molecule which is sufficiently energetic stretches and enters the interstices of the glass matrix. Once inside, the molecule may diffuse further, or it may dissociate into hydroxyl (OH^-) and ionic hydrogen (H^+) and react with the glass matrix. It then becomes immobile and does not diffuse further. In obsidian hydration, the concentration gradient driving the process is provided by the adsorbed water layer at the surface of the glass. Figure 3 shows a typical concentration profile of hydrogen ions as a proxy for water, measured by Secondary Ion Mass Spectrometry (SIMS); the curve moves to the right over time.

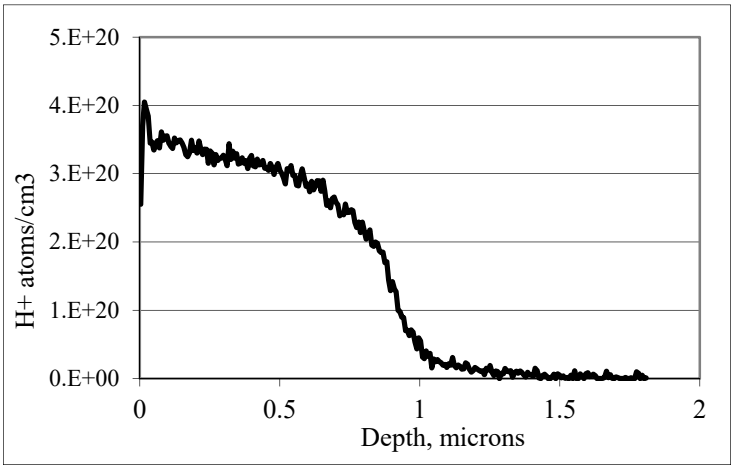

Figure 3. Typical profile for water diffusion in obsidian, using H^+ concentration as a proxy for diffused water. Note the "spike" in water concentration at the surface, representing adsorbed water and nano-fissures in the glass surface. Plot courtesy of Christopher M. Stevenson, Virginia Commonwealth University.

As the diffusion progresses, it causes a slight increase in the volume of the glass in the hydrated layer, which creates of a stress zone where it meets the unhydrated volume, which in turn causes a change in refractive index by the process of stress birefringence (Born and Wolf 1980: 703ff). If a small cross-sectional sample is cut from the obsidian, mounted on a microscope slide, and polished to transparency, the interface between hydrated and unhydrated volumes can be observed under a polarizing microscope. The hydrated volume is referred to as the hydration rim, and its thickness in archaeological cases is on the order of microns.

A property of any diffusion process is that a point on the concentration curve, say the 50% point, proceeds into the material at a rate which is proportional to the square root of time (Crank 1975; Rogers 2007a; Zhang 2008). Thus, if the point is the location of the observable hydration rim, then

$$r = \mathrm{sqrt}(t*k) \qquad (1)$$

where r is the hydration rim thickness in μ, t is time, and k is the hydration rate in μ^2/unit time.

A further property of the hydration rate is that it is a function of temperature by the Arrhenius equation (Doremus 2002)

$$k = k_0*\exp(-E/RT) \qquad (2)$$

where k_0 is the pre-exponential constant, E is the activation energy of the diffusion process, R is the universal gas constant (8.314 j/mol°K), and T is temperature in °K. For most obsidian, the value of E/R is on the order of 10000°K, and is a function of the intrinsic water content of the obsidian but not of temperature.

Archaeological temperatures vary annually, seasonally, and daily, so the

hydration rate of an obsidian artifact varies as well; a temperature increase of 10°C roughly doubles the rate. Since real-world temperature variation is complex, an effective hydration temperature (EHT) is defined to characterize its effect: *EHT is a single constant temperature which would cause the same hydration rim as the actual temperature history over the same period of time*. If an effective hydration rate is defined as the average rate over a period of time τ, then

$$k_e = (1/\tau)*\int [k_0*\exp(-E/RT)]\, dt \qquad (3)$$

where temperature T is a function of time. From this it follows that EHT is

$$k_e = k_0*\exp(-E/R*EHT) \qquad (4)$$

or

$$EHT = - E/[R*(\ln(k_e/k_0)] \qquad (5)$$

The numerical solution to these equations is discussed below under Module 5.

Code Details

Module 1: This module sets the constants to be used in computation. The parameter CVKE is an estimate of the coefficient of variation (CV) of the hydration rate ascribed to a source (not the same as the CV due to intrinsic water variation), and is set = 0.05 (Rogers 2010a). The parameter YBZ is the fraction of time as artifact was buried at the recovery depth, to account for site formation processes, and is set = 0.5 (Rogers and Yohe 2016). SIGEHT is the standard deviation of the EHT uncertainty due to meteorological modeling, and is set = 1°C (Rogers 2007a). EHTR is the EHT for the hydration date data and is set at 20°C.

Module 2: This module reads the input data from a .csv file. The user must adjust the filename in the csvread statement to match the name and path of the actual input file. The data fields are in Table 1.

Column	Definition
1	A sequence number assigned to each data point
2	The elevation of the archaeological site, in ft amsl.
3	The mean hydration rim reading for the specimen, in microns. This will be derived from the obsidian laboratory report.
4	The standard deviation of the rim reading, in microns. Most laboratories make and report six measurements of the rim, from which this parameter can be calculated. If not, using a value of 0.1μ is safe if N = 1. If a sample size N > 1 is used, this parameter is the standard deviation for the sample.
5	Burial (recovery) depth, in meters.
6	Sample size. I prefer to use N = 1 and aggregate the ages after computing them, but sometimes for debitage, larger samples are appropriate. Do not mix geochemical sources, however, nor provenience.
7	The geochemical source. Coso Sugarloaf Mountain = 1, Coso West Sugarloaf = 2, Coso West Cactus Peak = 3, Coso Joshua Ridge = 4, Bodie Hills = 5, Casa Diablo Sawmill Ridge = 6, Casa Diablo Lookout Mountain = 7, Queen = 8, Napa Glass Mountain = 9, Fish Springs = 10.
8	A flag variable (NOM), which tells the code which burial condition to use in computing the overall uncertainty. Usually set = 2, for the mixed case.

Table 1. Input data field definitions.

The most convenient way to create this file is in .xls format, then <save as> in .csv format. Note that it can contain numerical data only - no alpha characters. It is also important to be aware of a quirk of Excel here. In .xls format, the numerical values are saved to full precision, no matter what number format is selected; in .csv they are not, but are truncated by the format statement so precision is lost. It is a good idea to save the parameters with an extra figure after the decimal point, especially the rim standard deviation.

Module 3: This module computes obsidian activation energy from the hydration rate, to improve the accuracy of the EHT calculation. Hydration rate is defined by obsidian water content and effective hydration temperature, by the equation

$$k=\exp(37.76–2.289*w–10433/T+1023*w/T) \quad (6)$$

where k is hydration rate in $\mu^2/1000$ years at temperature T, and w is intrinsic total water content in wt%. Total water is the sum of molecular water and hydroxyl (Rogers 2015). Water content can thus be inferred from hydration rate and EHT by reversing this equation

$$w=[\ln(k)–(37.76–10433/EHT)]/(-2.289+1023/EHT) \quad (7)$$

and the activation energy in °K is

$$E/R = 10433 – 1023*w \quad (8)$$

This value of E/R is used in computing EHT, since it is a better estimate than the nominal 10000°K which is normally used. One outcome is that the computed value of EHT is a function of the obsidian source.

The module also sets the hydration rates to be used in the age calculation. Source data are: Coso (Rogers 2013a), Bodie Hills (Rogers 2013b), Casa Diablo and Fish Springs (Rogers 2017), Queen (Rogers 2016a), and Napa Glass Mountain (Rogers 2010b). Estimates of intra-source intrinsic water variation are from Stevenson et al. 1993 and Rogers 2008.

Module 4: This module contains the model relating site elevation to site temperature parameters for the high desert of eastern California. Three parameters are modeled: annual average temperature, annual temperature variation (hot-month mean minus cold-month mean), and mean diurnal variation. The model is based on 30-year data from thirteen weather stations in eastern California, ranging in elevation from 940 to 12,470 ft. above mean sea level (amsl), and the temperature parameters are computed from site elevation. The model equations are

$$Ta = 22.71 – 0.0020*h \quad (9a)$$

$$Va = 24.25 – 0.0006*h \quad (9b)$$

$$Vd = 18.49 – 0.0007*h \quad (9c)$$

where h is site elevation in feet (Rogers 2016b).

Further, it has been found for the desert case, that there is a consistent annual periodicity to the mean diurnal variation given by

$$V_d(t) = V_d + V_{da}*\cos(\pi m/6) \quad (10)$$

where m is the number of the month (1 – 12) and $V_{da} \approx 2.08$°C. A description of the analysis and resulting model is in Rogers 2016b, which has been uploaded on the IAOS website for ease of access.

A user working in another area could modify the model as needed or substitute another model.

Module 5: Module 5 is the core of the EHT calculation. Evaluating EHT (equation 5) requires first computing the effective hydration rate (equation 3), in which the temperature terms fluctuate according to a meteorological

model. Unfortunately, there is no known analytic solution to the integral in equation (3), so it must be solved by numerical integration.

The temperature history is modeled over the course of a year as

$$T = T_a + (V_a/2)*\cos(2\pi*n/(24*365)) + (V_d/2)*\cos(2\pi*n/24) \quad (11)$$

where T_a is the annual average temperature, V_a is the annual variation (hot-month mean minus the cold-month mean), and V_d is the mean diurnal variation. In addition, the computation of V_d includes the periodicity described by equation (10) above.

The method to evaluate effective rate is then

$$keff = (1/N)*\sum\{\exp[(-E/R)/T(n)] \quad (12)$$

where keff is the same as k_e in equation (3), T(n) is given by equation (11) with equation (10) substituted for V_d and the sum is taken over N = 24*365 = 8760 data points, i.e. one full year. (This is why it is impractical to implement the calculation in MS Excel – it would require a spreadsheet with 8760 lines, and would execute very slowly.) Finally, the EHT is

$$EHT = -(E/R)/\ln(keff) \quad (13)$$

Burial depth does not affect average annual temperature, but it progressively attenuates temporal variations (Carslaw and Jaeger 1959). Taking burial depth into account, the values of V_a and V_d are modified for attenuation with depth as

$$V_a = V_{a0}*\exp(-0.44*z) \quad (14)$$

and

$$V_d = V_{d0}*\exp(-8.5*z) \quad (15)$$

where V_{a0} and V_{d0} are the temperature variation at the surface derived from the meteorological model, V_a and V_d are the same parameters at burial depth, and z is burial depth in meters. The attenuation coefficients were measured for desert conditions (Rogers 2007b) and agree well with values for dry sand given in Carslaw and Jaeger (1959). Note that the attenuation factors in Rogers 2007a are incorrect and should not be used.

The code computes three cases: surface, burial depth, and mixed, which assumes the artifact was buried half its life and on the surface the other half (for YBZ = 0.5, module 1). The computation is

$$keff_m = YBZ*keff_s + (1-YBZ)*keff_d \quad (16)$$

where $keff_m$ is the mixed value, $keff_s$ is the value for surface conditions, and $keff_d$ is the value for burial depth z. Effective hydration temperature is then computed from equation (13) using $keff_m$.

Module 6: Module 6 uses the computed values of EHT to correct the measured hydration rim data to the EHT of the hydration rate, and then computes age based on the corrected rim. Note that all temperatures are in °K, not Celsius. The rim correction for EHT is

$$RCF = \exp\{[(E/R)/EHT_a - (E/R)/EHT_r]/2\} \quad (17)$$

where E/R was computed by equation (8), EHT_a is the EHT for the artifact, and EHT_r is the EHT for the hydration rate. The corrected rim value r_c is then

$$r_c = r_m*RCF \quad (18)$$

where r_m is the measured rim value, and the age is

$$t = r_c^2/k \quad (19)$$

where k is the rate. Again, the RCF, rim, and age are computed for three cases: surface, buried, and mixed.

The standard deviation of the measured rim is also adjusted for EHT as

$$\sigma_{rc} = \sigma_{rm} * RCF \quad (20)$$

where σ_{rm} is the measured standard deviation provided by the laboratory and σ_{rc} is the EHT-corrected standard deviation. In this case, only one value is computed, for the mixed case.

Module 7: Module 7 computes the best estimate of age uncertainty, based on a comprehensive model of error processes (Rogers 2010a). The primary sources of uncertainty or error are: obsidian rim measurement; errors in the hydration rate ascribed to a source, intra-source rate variability due to uncontrolled intrinsic water in the obsidian (Stevenson et al. 1993, 2000; Zhang et al. 1991; Zhang and Behrens 2000), errors in reconstructing the temperature history (Rogers 2007a), and burial depth errors caused by site formation processes (Schiffer 1987). Obsidian sample size in practical archaeological analyses is generally relatively small due to cost constraints, typically ~ 8-10, while the uncertainty sources produce at least five degrees of freedom in the errors. Thus, the sample standard deviation is a poor estimate of overall error. A better strategy for estimating age uncertainty is to use *a priori* information about the individual error sources and infer the accuracy of the age estimate.

This module computes these five uncertainties and outputs them for user study. The uncertainty variance due to laboratory measurement inaccuracy, Labvar,

$$Labvar = 4*(\sigma_r/r)^2 \quad (21)$$

where σ_r is the standard deviation of the laboratory measurement, and r is the corresponding rim value. The uncertainty variance due to EHT history is

$$EHTvar = 4*(0.06*\sigma_{EHT})^2 \quad (22)$$

where σ_{EHT} is the uncertainty in reconstructing a temperature history from modern records, and is ≈ 1°C. The uncertainty variance due to intra-source intrinsic water variation is

$$Watervar = 4*CVKS^2 \quad (23)$$

where CVKS is the CV of the intrinsic water content for the source. In the absence of measured data, a CVKS of 0.15 – 0.2 is reasonable. The uncertainty variance due to errors in the rate ascribed to a geochemical source is

$$Ratevar = 4*CVKE^2 \quad (24)$$

where CVKE is the CV of the rate ascribed to a source. The uncertainty is due to the fact that the rate must have been computed by some means, such as obsidian-radiocarbon association, and has uncertainty attached to it; a value of 0.05 was assigned in Module 1.

Finally, there is an uncertainty due to site formation processes which can change burial depth. The two limiting cases are the assumption that the artifact spent all its life on the surface, and the contrary assumption that it spent its life at the recovery depth. The age variance is then

$$SFvar = (t_s - t_d)^2/12 \quad (25)$$

where t_s and t_d are age assuming surface and depth conditions, respectively.

Note that SFvar is in years, while the other variances are ratios which must be multiplied by age to get an age variance. Thus the standard deviation of the overall age uncertainty (MODSD) is

$$MODSD = sqrt[(Labvar + EHTvar + Watervar + Ratevar)*t + SFvar] \quad (26)$$

where t is age. It is chosen from either surface case (NOM = 1), mixed case (NOM = 2) or burial case (NOM = 3).

Module 8: Module 8 creates the output data file in .csv format. The file is large, with 24 columns to aid the analyst in understanding the dominant processes. Most of the columns would not be reported in a practical archaeological report. The output format is as in table 2.

User Instructions

MatLab is an application system developed for scientific computation and engineering design. It is quite expensive, unless you have access to it via an institutional arrangement. Furthermore, use of this code requires familiarity with MatLab coding processes, which are not well documented. A reference I have found useful is Hunt et al. 2001. Other references are Higham and Higham 2000, Palm 2005, and Otto and Denier 2005. I have not found the Help menu to be especially helpful.

There are freeware alternatives to MatLab, for example, Gnu Octave and Freemat. I have tested the code on Gnu Octave, and it does execute, although not as quickly. Of course, the user still needs to be able to program in MatLab..

To use the MatLab code, go to the IAOS website and locate the file (it should be in .pdf format). Highlight the code, copy it, open MatLab, open a new m-file, and paste. (In Octave it is called a "script file" instead of a"m-file", but it works the same.) It is as simple as that. You will need to save it, and you can assign whatever name you like. Before using, you will need to modify the input and output filenames and paths to reflect your system. You can modify the temperature model, and create new geochemical sources. Good luck!

Column	Data Definition
1	Specimen sequence number
2	Site elevation, ft amsl
3	Annual average temperature, °C, computed from model
4	Annual temperature variation at the surface, °C, computed from model
5	Mean diurnal temperature variation at the surface, °C, computed from model
6	Surface EHT, °C
7	Measured mean value of hydration rim, μ
8	Standard deviation of lab measurements of rim,μ
9	Burial depth, meters
10	Sample size N
11	Geochemical source (number from Table 1)
12	Rim value corrected to EHT of the rate, μ
13	Rim standard deviation corrected to EHT of the rate, μ
14	Age for surface conditions, cal years before 2000
15	Age for depth conditions, cal years before 2000
16	Age for mixed conditions, cal years before 2000
17	Overall age uncertainty (equation (25)), cal years
18	Probable error of the mean, MODSD/sqrt(N)
19	Age variance due to rim reading
20	Age variance due to EHT uncertainty
21	Age variance due to intra-source intrinsic water variation
22	Are variance due to uncertainty in rate ascribed to source
23	Age variance due to site formation processes
24	Nominal condition flag value (NOM)

Table 2. Output data file column definitions.

References Cited

Born, M., and E. Wolf. (1980) *Principles of Optics: Electromagnetic Theory of Propagation, Interference, and Diffraction of Light,* 6th ed. Pergamon Press, New York.

Carslaw, H. S., and J. C. Jaeger (1959) *Conduction of Heat in Solids*, 2nd ed. Clarendon Press, Oxford.

Cole, F. W. (1970) *Introduction to Meteorology*. Wiley, New York.

Crank, J. (1975) *The Mathematics of Diffusion*. Oxford University Press, Oxford.

Doremus, R. H. (1994) *Glass Science*, 2nd ed. Wiley Interscience, New York.

Doremus, R. H. (2002) *Diffusion of Reactive Molecules in Solids and Melts*. Wiley Interscience, New York.

Higham, D. J., and N. J. Higham (2000) *MatLab Guide*. Society for Industrial and Applied Mathematics (SIAM), Philadelphia.

Hughes, R. E. (1988) The Coso Volcanic Field Reexamined: Implications for Obsidian Sourcing and Dating Research. *Geoarchaeology* 3: 253-265.

Hunt, B. B. (2001) *A Guide to MatLab for Beginners and Experienced Users.* Cambridge University Press, Cambridge.

Otto, S. R., and J. P. Denier (2005) *An Introduction to Programming and Numerical Methods in MATLAB.* Springer, London.

Palm, W. J., III (2005) *An Introduction to MatLab 7 for Engineers*. McGraw-Hill, New York

Rogers, A. K. (2007a) Effective Hydration Temperature of Obsidian: A Diffusion-Theory Analysis of Time-Dependent Hydration Rates. *Journal of Archaeological Science* 34: 656-665.

Rogers, A. K. (2007b) Attenuation of Temperature Variation with Depth in Desert Conditions. Maturango Museum Working Manuscript MS26. 19 August 2007.*

Rogers, A. K. (2008) Obsidian Hydration Dating: Accuracy and Resolution Limitations Imposed by Intrinsic Water Variability. *Journal of Archaeological Science*. 35: 2009-2016

Rogers, A. K. (2010a) Accuracy of Obsidian Hydration Dating based on Radiocarbon Association and Optical Microscopy. *Journal of Archaeological Science* 37: 3239-3246.

Rogers, A. K. (2010b) Laboratory Measurement of Hydration Rate for Napa Glass Mountain Obsidian. Maturango Museum Working Manuscript MS83, Rev C, September 13, 2010.*

Rogers, A. K. (2013a) Flow-Specific Hydration Rates for Coso Obsidian. *Proceedings of the Society for California Archaeology* 27: 281-294.

Rogers, A. K. (2013b) Computation of a Hydration Rate for Bodie Hills Obsidian, from Mono County, eastern California. Maturango Museum Working Manuscript MS66, Rev C, 12 June 2001.*

Rogers, A. K. (2015) An Equation for Estimating Hydration Rate of Obsidian from Intrinsic Water Concentration. *International Association for Obsidian Studies Bulletin* 53: 6-13.

Rogers, A. K. (2016a) A Physics-Based Hydration Rate for Queen Obsidian, Western Nevada. Maturango Museum Working Manuscript MS129, 6 June 2016.*

Rogers, A. K. (2016b) Regional Temperature Modeling for the Upper Mojave Desert. Maturango Museum Working Manuscript MS177, Rev C, 19 June 2016.*

Rogers, A. K. (2017) Hydration Rates for Casa Diablo and Fish Springs Obsidians, Eastern California. *International Association for Obsidian Studies Bulletin* 56: 5-10.

Rogers, A. K., and R. M. Yohe (2016) A Case Study in Site Formation Effects on Obsidian Hydration Dating. *International Association for Obsidian Studies Bulletin* 55: 5-9.

Schiffer, M. E. (1987) *Site Formation Processes of the Archaeological Record*. University of Utah Press, Salt Lake City.

Stevenson, C. M., E. Knauss, J. J. Mazer, and J. K. Bates (1993) The Homogeneity of Water Content in Obsidian from the Coso Volcanic Field: Implications for Obsidian Hydration Dating. *Geoarchaeology* 8(5): 371-384.

Stevenson, C. M., J. J. Mazer, and B. E. Scheetz (1998) Laboratory Obsidian Hydration Rates: Theory, Method, and Application. In M. S. Shackley (ed.) *Archaeological Obsidian Studies: Method and Theory. Advances in Archaeological and Museum Science*, Vol. 3, pp.181-204. Plenum Press, New York.

Stevenson, C. M., M. Gottesman, and M. Macko (2000) Redefining the Working Assumptions for Obsidian Hydration Dating. *Journal of California and Great Basin Anthropology* 22(2): 223-236.

Zhang, Y., E. M. Stolper, and G. J. Wasserburg (1991) Diffusion of Water in Rhyolitic Glasses. *Geochimica et Cosmochimica Acta* 55: 441-456.

Zhang, Y., R. Belcher, P. D. Ihinger, L. Wang, Z. Xu, and S. Newman (1997) New Calibration of Infrared Measurement of Dissolved Water in Rhyolitic Glasses. *Geochimica et Cosmochimica Acta* 61(15): 2089-3100.

Zhang, Y, and H. Behrens (2000) H_2O Diffusion in Rhyolitic Melts and Glasses. *Chemical Geology* 69: 243-262.

Zhang, Y. (2008) *Geochemical Kinetics*. Princeton University Press, Princeton.

*Working papers can be accessed via the IAOS website at www.peak.org/obsidian

REPORTING ON AN ADDITIONAL OBSIDIAN MACRO-CORE FROM BELIZE, CENTRAL AMERICA: MORPHOLOGY, GEOCHEMISTRY, AND SIGNIFICANCE

Lucas R. Martindale Johnson[a], Melissa Badillo[b, c], Nicholas Hamilton[d], and Silvia Batty[c]

a. Far Western Anthropological Research Group, Inc., b. University of Nevada, Las Vegas,
c. Institute of Archaeology, Belize, d. University of New South Wales (Australia)

Introduction and Background

Few large obsidian macro blade-cores have been recovered from ancient Maya archaeological sites far from quarry areas (i.e., consumer sites with local workshops). Most blade-cores recovered are typically small and usually exhausted, and of these, most are recovered from ritual contexts, not workshops. Many of these small, ritualized, exhausted blade-cores are typically modified (bi)laterally or otherwise systematically destroyed prior to deposition in a ritual context (see Johnson 2016 for examples). However, Thomas Hester (1972) reported on four macro-cores (only one of which was from a ritual cache), some with and without provenience, and discussed them in technological detail. In this report, we summarize those presented by Hester and describe another macro-core example that was recently re-discovered among curated artifacts in the Institute of Archaeology of Belize (IOA) curation facility. Macro-cores referred to herein can also be referred to as primary or as secondary macro-cores depending on the level of unidirectional, lateral, and radial percussion to shape the core. Kenneth Hirth and Bradford Andrews (2002: 2-3) describe primary macro-cores as formed by the lateral removal of decortication flakes and other larger macro-flakes, whereas secondary macro-cores are formed by further unidirectional and radial percussion flaking to remove macro-blades. These macro-blades may still retain some cortical surface. Secondary macro-cores most resemble the macro-core described below and elsewhere (Hester 1972).

The goals of this short report are (1) to showcase an otherwise underreported and not-often-found artifact, (2) link its technological morphology and specific geochemistry to those presented in Hester (1972), and (3) to briefly discuss the importance of these macro-cores in the overall production, distribution (exchange), and use of obsidian in the Maya Lowlands. In other words, the presence of these macro-cores at several sites beyond the quarry locations show material traces of the kinds of production and distributional relationships that existed between the Maya Highland and Lowland regions. In addition, the presence of these macro-cores reveals material evidence for what may have been traded through extensive land and sea trade routes. Although an exhaustive discussion of these last topics is beyond the scope of this report, we hope that greater attention will be paid to these types of artifacts and their implications for reconstructing the ancient Maya economic supply chain (Demarest et al. 2014: 188, Figure 1; Johnson 2016: 142, Figure 4-14; Nazaroff et al. 2010: 889, Figure 3).

The macro-core from Belize was analyzed during a research trip by one of the authors as part of dissertation research on obsidian from the site of Caracol, Belize (see Johnson 2016). During the trip, curated obsidian from Caracol was analyzed with a Bruker handheld portable ED-XRF instrument. Thus, we present on the macro-core's elemental composition, its source provenance, as well as general morphological dimensions and reduction extent/technique. Although the core currently lacks provenience information, it is likely from a site in Belize (John Morris, personal communication), and therefore may represent the first macro-core

Attribute	Papalhuanpa	Villahermosa	Quirigua	Tipuisate	IOA Belize
Height [Length] (cm)	19.2	22	16	24.9	17.4
Width	16.3	17	12.7	20	13.5
Max Diameter (striking platform)	16	15	12.2	20	13.5
Min Diameter (striking platform)	13.3	13	12	15.5	12.5
Weight (lbs.)	11	~13	4.9	27	nm
Blade scar length range	13.2-19.6	*-22	*-16	*-24.9	*-17.4
Blade scar width range	3.4-6.3	2.5-7.5	2-4**	2-5**	2-5**
Obsidian Source	no data	no data	Ixtepeque	El Chayal	Ixtepeque
Context	workshop	unknown	cache box	general excavation	unknown

*Note: *no minimum measurement available; ** inferred from images (Hester 1972:101, Figure 1); nm = not measured*

Table 1. General attributes from five obsidian macro-cores.

recovered from an eastern Lowland Maya site to the north of major quarry areas in highland Guatemala and sites near those quarries. To our knowledge, no other macro-core has been reported at known obsidian workshops in Belize (Olson 1994), and only one was reported from Tikal, Guatemala (Moholy-Nagy 2003: Figure 69a). Although essentially absent from Lowland Maya sites in the northern Petén or Belize, these macro-cores would have been traded in and through northern regions such as the Petén, Belize, and the Yucatan peninsula, as evidenced by the presence of larger percussion core-shaping debitage and (incised or bifacially worked) macro-blades (Coe 1965: 463, Figure 1a-i; Johnson 2016: 223, 226, Figure 5-32A; Moholy-Nagy 2003: Figure 68m; Sullivan 2017: 95, Figure 45), some of which contained cortex (Johnson 2016: 162, Figure 5-10).

Macro-cores Described by Hester (1972)

All but one of the cores described by Hester (1972) have archaeological provenience information and each core is described through morphological attributes (see Table 1 for a summary of these data). Each of the cores share generally similar attributes. The striking platform of each was created by splitting large nodules of obsidian as is evidenced by concentric percussion rings. Striking platforms were then modified by either faceting, grinding, or otherwise radial abrasion. Trimming also occurred around the striking platform to remove overhang material present from prior lateral blade/flake removal. Each core had up to 10 negative macro-blade scars. As a result of these blade removals, the cores became cylindrical, conical, or bullet-shaped. Large lateral blades could then be removed to form blade blanks for biface production. The crushing and battering on the distal end of at least one core suggests it was positioned on an anvil during hard/soft hammer percussion.

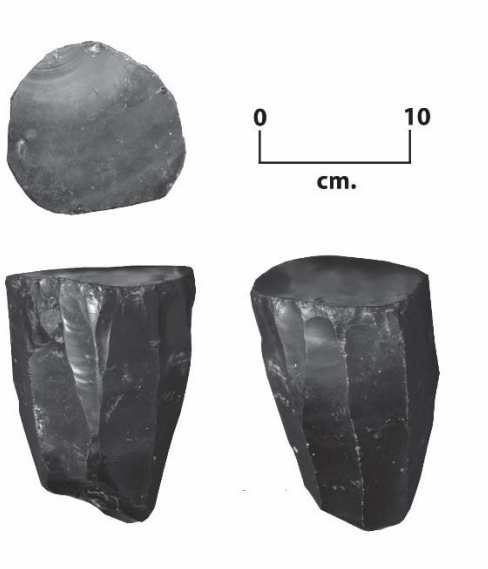

Figure 1. Three views of the IOA macro-core. Counter-clockwise from top: view of striking platform and lateral views.

IOA Macro-Core Morphology

The IOA macro-core shares most of the details described by Hester (1972). The striking platform, measuring 13.5 x 12.5 cm, was initially formed by the splitting of a nodule or

the removal of a large flat flake by direct percussion (Figure 1). After this procedure, the core was shaped by laterally or radially removing more than eight blades and flakes to form a slightly conical shape. This process likely removed any remaining cortical material. As inferred from the photographs, these blades would have been between two and five centimeters in width and at up to 17.4 centimeters long. There is no evidence showing removal of blades in a bidirectional manner. After this shaping process, the margins of the core's platform were retouched to remove any overhangs from prior flake/blade removal. This is evident by the short negative scars over top of the prior blade scars. The distal end of the core shows a large cone of force from an excessive impact (Figure 2). This could have happened by it being reduced on an anvil, but could have also occurred if it was dropped at some point during transport in antiquity or more recently. In either case, the distal end of the negative blade scars was removed during this event, therefore the core was likely about 2-5 centimeters longer that it is currently.

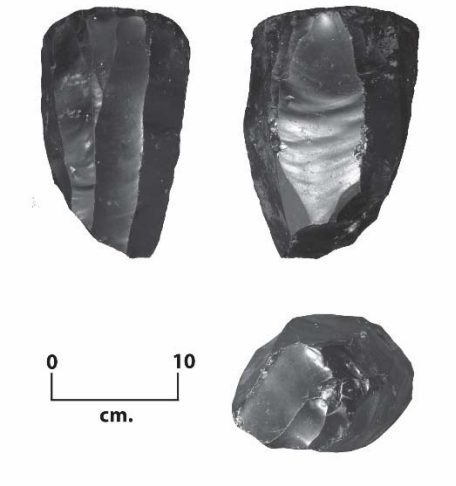

Figure 2. Three views of the IOA macro-core. Clockwise from top: lateral views and distal view (note the large cone of force).

Figure 3. ED-XRF scan of IOA macro-core using a Bruker Tracer III, Serial Number K0729

Elemental Concentrations from Handheld Portable XRF: Methods and Data

The core was analyzed with a Bruker Tracer handheld portable ED-XRF instrument (serial number K0729) that is currently managed by the University of Florida Anthropology Department (Figure 3). This instrument has a pin-diode detector and was operated at 40kV and 28μA for 180 live seconds. The 'green' filter was used to characterize elemental intensities for the K-alpha peaks of manganese (Mn), iron (Fe), zinc (Zn), gallium (Ga), rubidium (Rb), strontium (Sr), yttrium (Y), zirconium (Zr), and niobium (Nb), and the L-alpha peaks of thorium (Th). Trace-element peak intensities for the above elements are normalized to the Compton scatter peak of rhodium (19.5-22 keV) and converted to parts per million using the MURR 2 matrix-specific calibration, developed by Bruker

Elemental in collaboration with the University of Missouri Research Reactor (MURR, see Glascock and Ferguson 2012; Speakman 2012). This factory-installed calibration is based on analysis of 40 samples of unmodified obsidian and fine-grained volcanic rock from around the world, chosen to represent the range of trace-element concentrations known to occur in these materials. In addition to the core and other artifacts being scanned during the IOA visit, a USGS standard RGM-2 pressed pellet was also scanned. The reporting of ppm for the RGM-2 pressed pellet sample provides ppm concentrations for an independent international standard not currently part of the MURR 2 calibration algorithm. This reporting convention should help to provide a correspondence between alternative XRF analyses (Speakman and Shackley 2012).

XRF data from the core shows that it is made of Ixtepeque obsidian from the highlands of Guatemala. It was sourced by comparison to a thirteen-source comparative collection provided by MURR for the above-mentioned dissertation project albeit scanned on another Tracer XRF, Serial Number T3S1330 currently managed by the Archaeological Research Facility (ARF) at the University of California, Berkeley (Johnson 2016: 108, Figure 4-1). Elemental concentrations (ppm) and gross photon count percentages for the core, the MURR source material, and the RGM-2 pressed pellet are provided in Table 2. Initial analysis, however, using two elements (Sr and Zr) indicate it could be made of obsidian from the Otumba source in Mexico or from Ixtepeque obsidian in Guatemala (Figure 4). Though given the near overlap of the Ixtepeque and Otumba source material using only two elements (i.e., one Otumba obsidian source has higher Sr concentrations), alternative analysis using relative gross peak photon intensities percentages of Rb, Sr, and Zr were used to determine that the core is made of Ixtepeque obsidian (Figure 5).

This second semi-quantitative method of analysis is not typically used to source obsidian artifacts from Mesoamerica, but is commonly used to source small/thin (<4 x 4mm) artifacts from archaeological contexts in California and the Great Basin (see Hughes 2010 for an explanation of this analytical method). The overall size of these small/thin artifacts do not cover the entire detector window on Bruker Tracer XRF instruments (3 x 4mm) (see Ferguson 2012), thus they return low overall photon counts and thus once converted to ppm, do not entirely match thick and wide geological source reference material (see elongated plots in Johnson 2016:112-113). Although the core clearly covers the entire detector window (Figure 3), its ppm concentrations are more varied than the five Ixtepeque source samples provided by MURR, thus, other analyses were necessary to differentiate between the Otumba and Ixtepeque source material. The ternary plot provides a three-dimensional approach that works regardless of overall artifact size to separate those sources that may overlap in two-dimensional biplots. The use of a ternary diagram analysis method is easily adapted to other regional analyses and in particular provides a helpful way of characterizing very thin (1-3mm) blades commonly occurring in Mesoamerican archaeological contexts (see Johnson 2016: 113-114). Relative elemental percentages are calculated by taking the sum value of Rb, Sr, and Zr and dividing each individual value by the sum, thus calculating the percentage of each element relative to the sum (e.g., Rb / (Rb + Sr + Zr)).

In the absence of gross photon counts (uncorrected, not adjusting for inter-elemental effects) or net photon counts (corrected, adjusted for inter-elemental effects), which are usually not archived or published, the analyst can use the relative percentages of ppm concentrations with some caveats. Simply following the same above outlined procedure will produce comparable percentage relationships that can be graphed using a

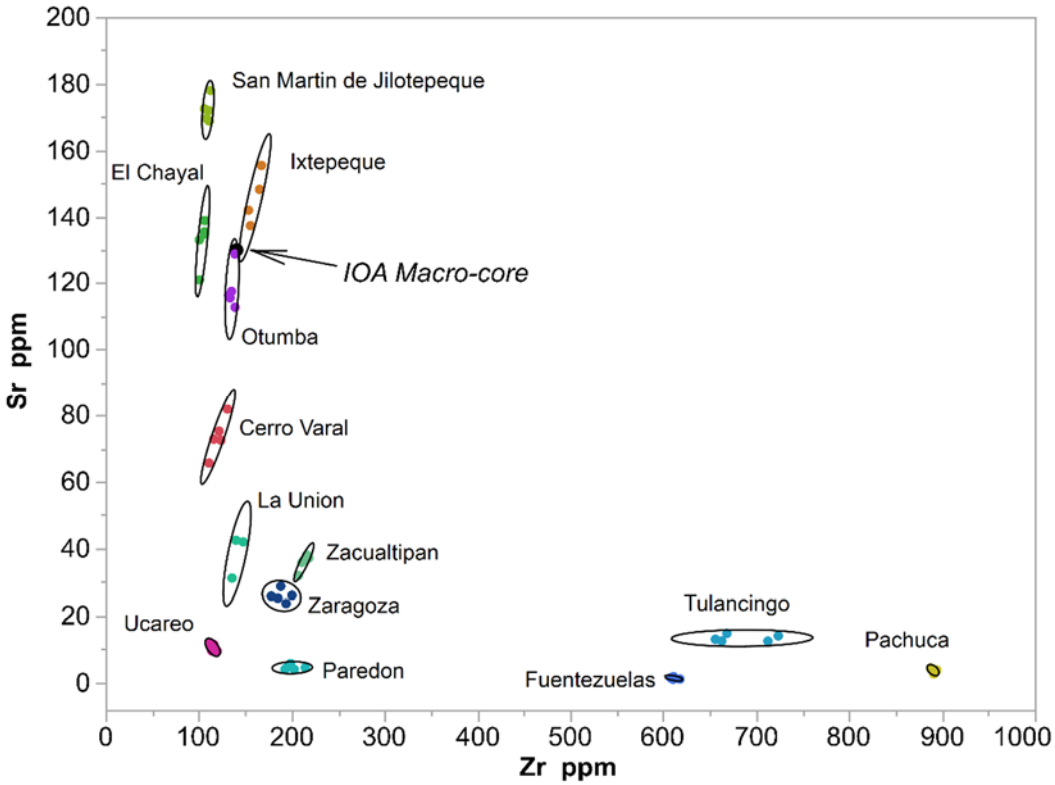

Figure 4. Sr by Zr ppm biplot with source data, their associated 95% confidence ellipses, and the IOA macro-core.

ternary diagram (see Johnson 2016: 113-114). In this report we use uncorrected gross photon counts. After the relative peak percentages were calculated (see Hughes 2010), the biplot and ternary diagram presented here were created using a combination of statistical programs and packages (ggtern [Hamilton 2018] in R [2017], and biplots in SAS JMP 13.0). The uncorrected gross photon counts are accessible during the calibration process using the S1PXRF Microsoft Excel macro add-in under the "PDZ file" tab, while net photon counts can be calculated through Bayesian modeling processing in Artax. After gross photon counts were copied and transformed to relative percentages, the macro-core and obsidian source data were plotted using the R package ggtern. The R package ggtern (Hamilton 2018) is a unique data analysis tool used to calculate statistical multinomial confidence regions for grouped source rock (Figure 5). The 95% confidence regions are calculated using the Mahalanobis distance (Mahalanobis 1936), operating on data that has been firstly transformed using the Isometric Log-Ratio transformation (Aitchison 1986). This transformation achieves a decomposition of the simplex (i.e., ternary diagram), as a vector space, into orthogonal subspaces (Egozcue et al. 2003) which therefore permit straightforward handling of geometric elements in the simplex. Other descriptions of calculating multinomial confidence regions can be found in Medak and Cressie (1991), Tolosana-Delgado et al. (2011), Watson (1997), Watson and Nguyen (1995), and Weltje (2002).

		Element PPM							Gross Photon Count Calculations			
Specimen	N=	Mn	Fe	Rb	Sr	Y	Zr	Nb	∑ Rb, Sr, Zr	Rb%	Sr%	Zr%
Cerro Varal	5											
Mean		404	6987	128	74	23	121	17	6684	0.318	0.230	0.452
Std Dev		49	471	5	6	2	8	0	198	0.010	0.004	0.009
El Chayal	5											
Mean		603	6155	140	133	19	104	11	7627	0.300	0.343	0.357
Std Dev		115	209	5	7	2	3	1	340	0.005	0.007	0.003
Fuentezulas	5											
Mean		206	14345	171	1	97	611	34	17477	0.156	0.012	0.833
Std Dev		75	203	4	0	1	4	2	179	0.003	0.001	0.003
Ixtepeque	4											
Mean		419	9149	100	146	18	161	10	8285	0.191	0.329	0.480
Std Dev		37	257	2	8	1	7	0	290	0.007	0.004	0.006
La Union	3											
Mean		451	7920	130	38	24	141	16	6605	0.332	0.134	0.534
Std Dev		143	434	12	6	4	6	2	381	0.007	0.012	0.014
Otumba	5											
Mean		401	8866	124	118	22	136	12	7729	0.259	0.299	0.443
Std Dev		23	364	5	6	1	3	1	239	0.006	0.010	0.005
Pachuca	5											
Mean		1050	15709	194	4	109	891	88	24428	0.126	0.010	0.863
Std Dev		79	180	2	1	3	3	1	313	0.001	0.001	0.002
Paredon	5											
Mean		364	8776	165	4	48	201	41	7608	0.347	0.030	0.623
Std Dev		28	317	7	1	3	9	2	194	0.002	0.002	0.004
San Martin de Jilotepeque	5											
Mean		553	6510	109	172	15	110	9	8284	0.222	0.411	0.366
Std Dev		28	153	4	4	2	3	1	392	0.004	0.005	0.004
Tulancingo	5											
Mean		435	18443	126	13	93	685	46	18046	0.108	0.022	0.870
Std Dev		47	706	5	1	4	31	1	790	0.004	0.001	0.004
Ucareo	5											
Mean		208	7569	150	10	26	115	14	5625	0.447	0.061	0.491
Std Dev		17	120	6	1	1	3	1	133	0.005	0.004	0.008
Zacualtipan	5											
Mean		183	10584	282	36	46	213	19	10317	0.429	0.079	0.491
Std Dev		26	551	9	2	2	4	1	75	0.007	0.003	0.005
Zaragoza	5											
Mean		263	9595	138	26	32	189	17	7231	0.302	0.084	0.614
Std Dev		29	343	5	2	2	8	1	159	0.005	0.005	0.009
RGM-2 (measured)	8											
Mean		220	11745	135	93	24	200	9	-	-	-	-
Std Dev		114	495	5	4	2	4	1	-	-	-	-
RGM-2 (recommended)										-	-	-
Actual		273	-*	147	108	24	222	9	-	-	-	-
Std Dev		8	-	5	5	2	17	-	-	-	-	-
UNPROV OBS CORE		387	9452	85	130	16	141	9	6319	0.179	0.327	0.495

Note: USGS reports Fe as an oxide, not ppm.*

Table 2. Elemental concentrations and relative photon percentages for obsidian sources and the IOA macro-core.

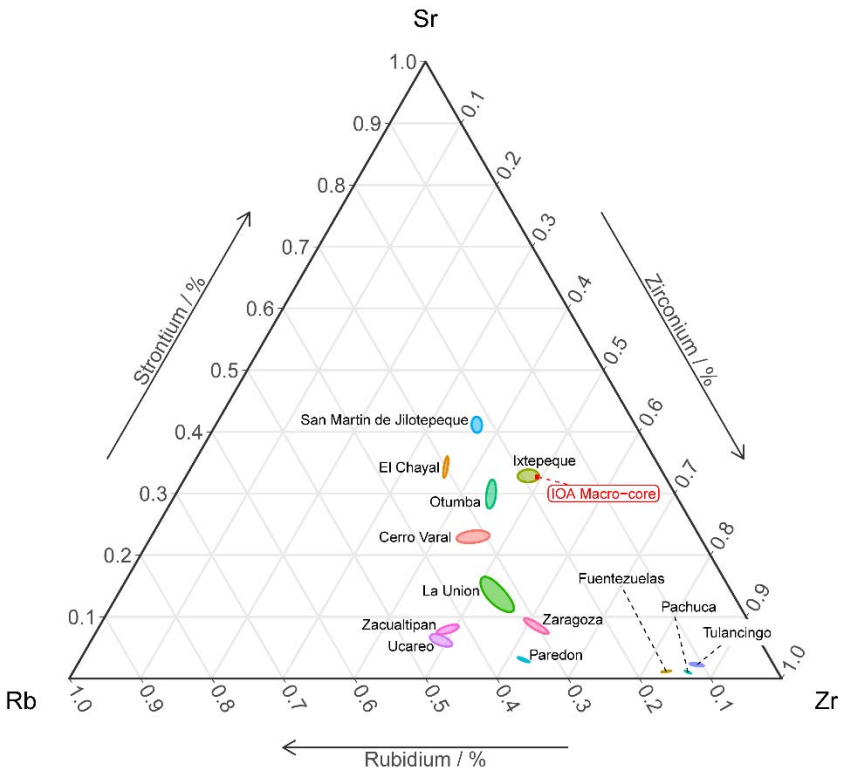

Figure 5. Ternary plot diagram of source samples and the IOA macro-core. Colored ellipses represent 95% multinomial confidence regions.

Implications

Technological analysis of the macro-cores shows a fairly standard practice in reduction across the handful of known examples. This practice included splitting large nodules and then abrading or otherwise preparing striking platforms in a radial manner where large macro-blades or elongated flakes were removed. The distal ends of cores were also prepared slightly to create a tapered or cone shape. At least two of the cores described here show evidence of distal crushing, suggesting that cores were positioned on anvils when struck with direct or indirect percussion.

Thus far, few larger macro-cores have been recovered from Maya archaeological sites far from primary quarry areas, yet research on obsidian distributions and technological analysis shows cores, such as the one described here and elsewhere (Hester 1976) would have circulated widely. The indirect evidence of this circulation is demonstrated by the presence of large macro-blades and macro-flakes, both with and without cortex. These macro pieces of debitage were driven off macro-cores and further knapped to form larger bifaces or larger blade tools, both of which do show up in some ritual caches (Johnson 2016: 226, Figure 5-32; Moholy-Nagy 2003, Figure 68m) or in workshop dumps (Moholy-Nagy 1997: 304; Olson 1994: 24). Therefore, insofar as the archaeological record in the Maya Lowlands might typically lack complete macro-cores, there is some indirect evidence that suggests obsidian was initially quarried then shaped into primary macro-cores or secondary macro-cores that were then widely circulated to sites as far afield as those in present day Chiapas, Mexico, and Belize. These macro-cores being the starting point for pressure blade production in the Maya Lowlands were then reduced further, producing macro-blades, and then pressure blades with occasional rejuvenation when necessary. Scholars have modeled these

reduction processes (Hirth and Andrews 2002) and distributional trade routes with varying levels of detail (see Demarest 2014), but all would likely agree that the itinerary of macro-cores originating in the Guatemalan highlands, conveyed by well-connected merchants, would have included passage through many cities and hamlets on the way northward into the ancient Maya Lowlands. Based on the abundance of obsidian excavated from ancient Maya sites, the movement of macro-cores was likely a regular process.

In prior research, emphasis had been placed on the connectivity of different regions, each with important and unique resources (Scarborough and Valdez 2009). The presence of this Ixtepeque core in comparison to another Ixtepeque core and a single sourced El Chayal core (Hester 1976) suggests a level of continuity in technique between those working at spatially separate quarries. In addition, it shows that both sources circulated widely in similar form, albeit in different quantities through time (Nazaroff et al. 2010). These data help to deepen our understanding of what was actually transported across vast land and water exchange routes for more than a millennium in the Maya area. The analysis of these macro-cores also enables archaeologists to understand how the blade-making process began at sites further afield.

Acknowledgements

We would like to thank the IOA for allowing the presentation of this core. In particular, we acknowledge the critical support of Dr. John Morris, Antonio Beardall, Josue Ramos, Paul Smith, and Sigourney Allen for providing access, photographs, and overall measurements on the obsidian core. Funding for the visit to the IOA was provided the National Science Foundation (award #1556260) and access to obsidian source material was provided by Mike Glascock and Jeff Ferguson of MURR (Missouri University Research Reactor). Lastly, this short report would not have been possible without support from Nico Tripcevich and Rosemary Joyce and a review of the manuscript draft by Brian Byrd.

References Cited

Aitchison, J. (1986) *The Statistical Analysis of Compositional Data*. Chapman and Hall, London.

Coe, W.R. (1965) Caches and Offertory Practices of the Maya Lowlands. In Willey G.R. and Wauchop, R., (eds.) *Handbook of Middle American Indians: Archaeology of Southern Mesoamerica, Part One*, pp. 462-468, University of Texas Press, Austin.

Demarest, A.A., Andrieu C., Torres, P., Forné, M., Barrientos, T., and Wolf M., (2014) Economy, Exchange, and Power: New Evidence from the Late Classic Maya Port City of Cancuen. *Ancient Mesoamerica* 25(1): 187-219.

Egozcue, J.J., Pawlowsky-Glahn, V., Mateu-Figueras, G., and Barcelo-Vidal, C. (2003) Isometric Logratio Transformations for Compositional Data Analysis. *Mathematical Geology* 35(3): 279-300.

Ferguson, J. (2012) X-Ray Fluorescence of Obsidian: Approached to Calibration and the Analysis of Small Samples. In A. N. Shugar and J. L. Mass (eds.) *Studies in Archaeological Sciences: Handheld XRF for Art and Archaeology*, pp. 401-422. Leuven University Press, Belgium.

Glascock, M. D. and J. Ferguson (2012) *Report on the Analysis of Obsidian Source Samples by Multiple Analytical Methods*. Report prepared for Bruker and available online: https://www.bruker.com/fileadmin/user_upload/8-PDF-Docs/X-rayDiffraction_ElementalAnalysis/HH-XRF/LabReports/Obsidian_Source_Samples.pdf

Hamilton, H. (2018) ggtern: An Extension to 'ggplot2' for the Creation of Ternary Diagrams. R package version 2.2.2. https://CRAN.R-project.org/package=ggtern

Hester, T.R. (1972) Notes on Large Obsidian Blade Cores and Core-Blade Technology in Mesoamerica. *Contributions of the University of California Archaeological Research Facility* 14, pp. 95-105. Berkeley.

Hirth, K. G., and B. Andrews (2002) Pathways to Prismatic Blades: Source of Variation in Mesoamerican Lithic Technology. In K. Hirth and B. Andrews (eds.) *Pathways to Prismatic Blade: A Study in Mesoamerican Obsidian Blade-Core Technology*, Monograph 45, pp.1-14. University of California, Los Angeles.

Hughes, R. E. (2010) Determining the Geologic Provenance of Tiny Obsidian Flakes in Archaeology Using Nondestructive ED-XRF. *American Laboratory* 42(7): 27-31.

Johnson, L. R. M. (2016) Toward an Itinerary of Stone: Investigating the Movement, Crafting, and Use of Obsidian from Caracol, Belize. Unpublished Ph.D. dissertation, University of Florida.

Mahalanobis, P. C. (1936) On the Generalized Distance in Statistics. *Proceedings of the National Institute of Sciences (Calcutta)* 2: 49-55.

Medak, F. and N. Cressie (1991) Confidence Regions in Ternary Diagrams Based on the Power-Divergent Statistics. *Mathematical Geology* 23(8): 1045-1057.

Moholy-Nagy, H. (1997) Middens, Construction Fill, and Offerings: Evidence for the Organization of Classic Period Craft Production at Tikal, Guatemala. *Journal of Field Archaeology* 24(3): 293-3136.

Moholy-Nagy, H. (2003) *The Artifacts of Tikal: Utilitarian Artifacts and Unworked Material*. Tikal Report No. 27 Part B. University of Pennsylvania Museum, Philadelphia.

Nazaroff, A. J., Prufer, K. M., and Drake, B. L. (2010) Assessing the Applicability of Portable X-ray Fluorescence Spectrometry for Obsidian Provenance Research in the Maya Lowlands. *Journal of Archaeological Science* 37(4): 885-895.

Olson, K. A. (1994) Inclusive and Exclusive Mechanisms of Power: Obsidian Blade Production and Distribution Among the Ancient Maya of the Belize River Area. Unpublished Master's thesis, University of California, Los Angeles.

R Core Team (2018) *R: A Language and Environment for Statistical Computing.* R Foundation for Statistical Computing, Vienna, Austria. URL http://www.R-project.org/.

Scarborough, V. L., and F. Valdez (2009) An Alternative Order: The Dualistic Economies of the Ancient Maya. *Latin American Antiquity* 20(1): 207-227.

Speakman, R. J. (2012) *Evaluation of Bruker's Tracer Family Factory Obsidian Calibration for Handheld Portable XRF Studies of Obsidian*. Prepared for Bruker AXS, Kennewick, Washington.

Sullivan, K. J. (2017) Caching It In: Local Patterns in Ancient Maya Ritual Caches of Eccentric Lithics within the Belize Valley. Unpublished Master's Thesis, Northern Arizona University.

Tolosana-Delgado, R., and K. G. van den Boogaart (2011) Linear Model with Compositions in R. In V. Pawlowsky-Glahn and A. Buccianti (eds.) *Compositional Data Analysis,* pp. 356-371, Wiley and Sons, West Sussex, U.K.

Watson, G.S. (1997) Letter to the Editor: Confidence Regions in Ternary Diagrams 2. *Mathematical Geology* 19(4): 347-348.

Watson, G.S. and H. Nguyen (1985) A Confidence Region in a Ternary Diagram and Point Counts. *Mathematical Geology* 17(2): 209-213.

Weltje, G. J. (2002) Quantitative Analysis of Detrital Modes: Statistically Rigorous Confidence Regions in Ternary Diagrams and their Use in Sedimentary Petrology. *Earth-Science Reviews* 57: 211-253.

POVERTY POINT'S OBSIDIAN*

Diana M. Greenlee[a], Richard E. Hughes,[b] and Thomas M. Origer[c]

a. Poverty Point Station Archaeology Program and the University of Louisiana at Monroe, b. Geochemical Research Laboratory, c. Origer's Obsidian Laboratory

*This article previously published in Louisiana Archaeology 37: 89-107.

Abstract

In 1985, an obsidian fragment was collected from the ground surface along the eastern edge of Macon Ridge in the area of the northern ridges at Poverty Point (16WC5). Until 2009, this was the sole piece of obsidian known from the site and it was considered evidence for a westward extension of the Poverty Point trade network into Wyoming. During construction of a maintenance building on the park north of Harlin Bayou in 2009, three more pieces of obsidian were recovered from near-surface contexts. This prompted reconsideration of the role of obsidian in Poverty Point culture. X-ray fluorescence and neutron activation analyses were used to examine the geochemical sources of the fragments. Two of the fragments are from the Glass Buttes Complex (Oregon) and two are from unknown sources. Obsidian hydration analysis showed no hydration band formation, leading us to conclude that modern flintknappers brought the obsidian to Poverty Point.

Introduction

With its monumental earthworks, Poverty Point (16WC5) in northeast Louisiana is the largest and most complex Late Archaic site in North America (Figure 1). The designed landscape includes five earthen mounds (Mounds A, B, C, E and F) and six, concentric, semi-elliptical, earthen ridges surrounding a huge, leveled, 17.4 ha plaza. Its construction required an enormous labor investment, estimated at 1.5 million cubic meters of soil movement if one includes landscape preparation (filling gullies and leveling high spots), on the part of the hunter-fisher-gatherers who built and occupied the site ca. 3,700–3,100 B.P. (Connolly 2006). A sixth mound (Mound D) was added to the complex about 1,700–2,000 years later.

Poverty Point is also unusual because of the abundance of exotic raw materials in its lithic assemblage. Most of the exotic stone is from sources 250–900 km away, with some from as far away as 1,600 km (Gibson 1994). Even the "local" rock was brought in from over 40 km away. The lithic assemblage at Poverty Point is not just a few boxes of stone. Rather, the amount of rock at the site has been estimated to be over 71 metric tons (Gibson 1994). Efforts are ongoing to determine where some of Poverty Point's raw materials came from. Copper, for example, has long been assumed to have come from Great Lakes sources, but recent analyses suggest other sources are likely (Hill et al. 2010). Pumice may have been collected from Louisiana beaches, deposited by Gulf of Mexico currents after transport from volcanoes probably in the Lesser Antilles of the Caribbean (Greenlee 2009), although some pumice-like fragments may be clinker from the Ft. Union Formation in North Dakota that floated down the Missouri and Mississippi Rivers. Poverty Point's obsidian, until now, was believed to have come from Wyoming (Gibson 2000).

Beyond Poverty Point, there are a limited number of obsidian artifacts known from archaeological sites in the southeastern United States. Several of these have been characterized as to their trace element composition and their likely geochemical source (Table 1). For many of these artifacts, hydration rind thickness is consistent with a prehistoric origin. Unfortunately, they are not all from secure archaeological contexts that

State	Site Name & Number	Time Period	Artifact	Hydration Band Thickness (μm)	Geological Source	Reference
AL	1LI34	Multi-Component	Point	3.0	Coglan Buttes, OR	Norton 2008
AL	Moundville 1TU500	Late Prehistoric	Point	-	Grasshopper Group, CA	Hammerstedt et al. 2010
AL	Moundville 1TU500	Late Prehistoric	Point	-	uncertain	Hammerstedt et al. 2010
AR	Brown Bluff 3WA10	Intrusive?	Flake	-	Malad, ID	Hughes et al. 2002
LA	Cross Lake 16CD118	Multi-Component	Uniface	-	uncertain	Jeane 1984
LA	Doug Schultz	-	Core	-	Obsidian Ridge, NM	Skinner 2007
MS	Myer 22CO529	Multi-Component	Point	2.3 ± .1	Malad, ID	Peacock et al. 2006
MS	Parker Bayou II 22HO626	Multi-Component	Point	3.2 ± .1	Obsidian Ridge, NM	Peacock et al. 2006
TN	40BN58	Archaic	Flake	6.1	Sarcobatus Flat A, NV	Norton 2008
TN	40CH26	Archaic	Point	4.2	Napa Valley, CA	Norton 2008
TN	40DV194?	Multi-Component	Point	6.2 ± .1	Obsidian Cliff, WY	Braly and Sweat 2008
TN	40HS48	Multi-Component	Flake	1.6	Government Mtn, AZ	Norton 2008
TN	40SW186	Archaic	Point	1.4	Annadel, CA	Norton 2008
TN	40SW186	Archaic	Point	1.4	Napa Valley, CA	Norton 2008
TN	40WM63	-	Flake	Modern	Western Mexico	Norton 2008
TN	No site #	-	Point	2.8	Napa Valley, CA	Norton 2008

Table 1. Source assignments from trace element analysis of obsidian artifacts in the southeastern United States.

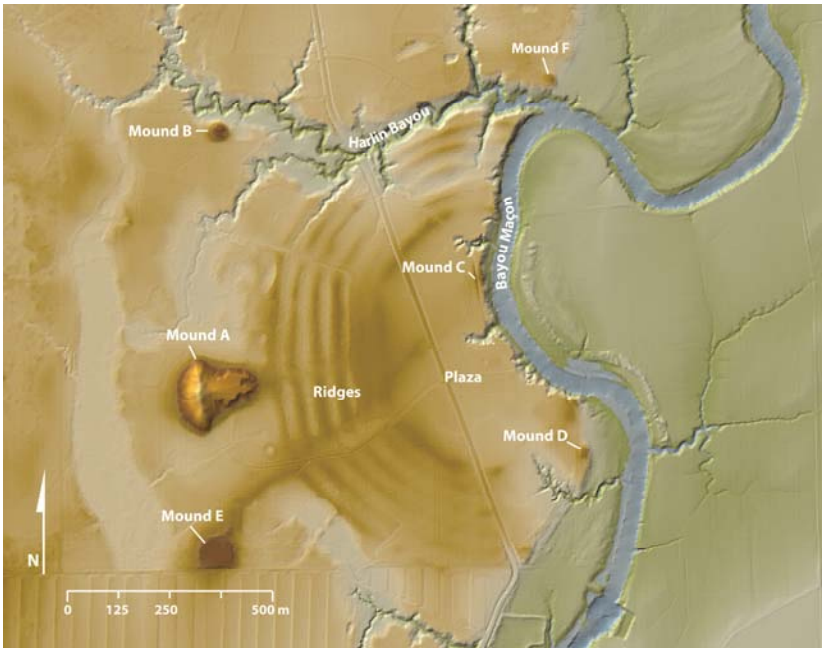

Figure 1. LiDAR (Light Detection and Ranging) map of Poverty Point. LiDAR data courtesy of the State of Louisiana and FEMA, distributed by "Atlas: The Louisiana Statewide GIS," LSU CADGIS Research Laboratory, Baton Rouge, Louisiana.

would convincingly support a prehistoric introduction into the region and they could represent modern contamination. Still, these occurrences lend plausibility to the idea that obsidian could have been acquired by the people of Poverty Point.

Background

In 1985, a piece of obsidian was collected by Jon Gibson on the surface at the eastern end of Ridge 4 North (Figure 2). Gibson recollects that the fragment was found with other artifacts typical of the Poverty Point occupation on the surface of a "slump block washed downslope from the end of the N4-bank of Bayou Maçon" (personal communication, 2010). The roughly 2.4 × 2.6 × .4 cm piece, referred to here as PP-1, resembles a large blade midsection, with some apparent "nibbling" along one edge (Figure 3). Until recently, PP-1 was the only piece of obsidian known from Poverty Point.

Gibson sent PP-1 to one of us (Hughes) in 1988 for energy dispersive x-ray fluorescence (XRF) analysis. PP-1 did not match any of the laboratory's geochemical sources from North America or Mesoamerica. The first published reference about the obsidian in 1990 (Gibson 1990: 261) cites that inability to determine a source; however, in 1999, the obsidian came from "out West somewhere" (Gibson 1999: 58). By 2000, the notion that the obsidian fragment came from an unidentified source in Wyoming was introduced (Gibson 2000: 173, 270). This apparent change in provenance occurred even though no additional analyses were conducted on the piece. With Wyoming ("resembles Wyoming material but is definitely not from Yellowstone" [White and Weinstein 2008: 235]) or "an undisclosed source in the Rockies" (Gibson 2010: 81) as the currently accepted geological source for PP-1, that single piece of obsidian represented a significant westward expansion of the vast Poverty Point exchange network (Anderson et al. 2007; Anderson and Sassaman 2009).

Three more obsidian fragments, referred to here as PP-2, PP-3 and PP-4, were found during construction of a new maintenance building (Figure 4) north of Harlin Bayou in 2009 (Greenlee 2009). PP-2 was recovered from the backdirt pile produced when a subcontractor mechanically scraped the sod from the construction area; later, PP-3 and PP-4 were recovered when surface sediments were shovel-scraped prior to mechanical trenching for a sewer line. PP-2 appears to be a biface fragment, PP-3 looks like shatter, and PP-4 is clearly a flake fragment (Figure 5).

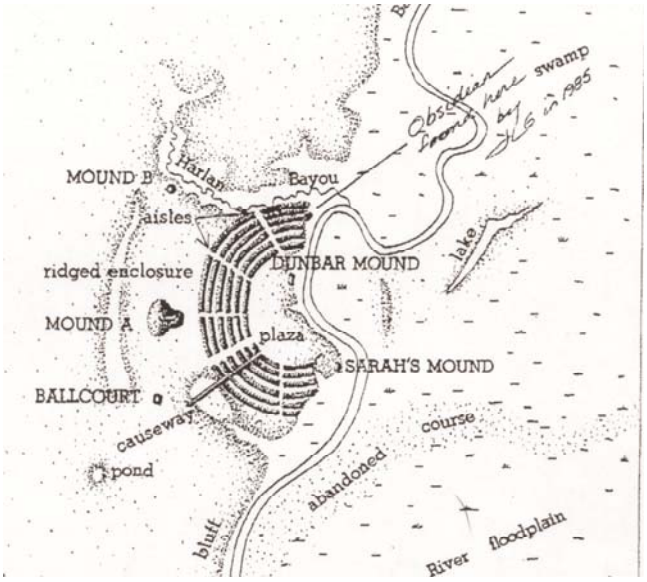

Figure 2. Location of obsidian fragment PP-1 as recorded by Jon Gibson.

Figure 6 shows the complete assemblage of obsidian artifacts recovered from Poverty Point.

The three most recently-discovered pieces, representing 75% of the obsidian assemblage at Poverty Point, were all recovered using ⅛" screens. If they are representative of the size distribution of the obsidian at Poverty Point, it should be no surprise that only one piece had been found prior to this, since the vast majority of archaeological excavations at Poverty Point have relied on screens with ¼" or greater mesh size. The frequency of artifacts north of Harlin Bayou is quite low compared with that of the site core, located south of Harlin. Thus, it was surprising from a sampling perspective to recover so many specimens of an apparently rare material in an area of extremely low artifact density.

Figure 3. Obsidian fragment PP-1, with close-up showing "nibbling."

Unfortunately, the maintenance building fragments (PP-2, PP-3, and PP-4) are not from secure prehistoric contexts. There has been a significant amount of mixing in the area due to maintenance-related activities. In addition, these obsidian pieces were found near the long-term location of the park's dumpster. Debris from modern knapping activities has been known to escape the dumpster through the efforts of raccoons in search of food scraps and through the garbage transfer process. Obsidian, while not the most frequently worked stone, is used in knapping workshops at the park; most recently, knapper's obsidian was obtained from the Glass Buttes Complex in Oregon.

Methods

Energy Dispersive X-Ray Fluorescence

X-ray fluorescence (XRF) is one of the most commonly used methods for characterizing the chemical composition of obsidian. It has the advantage of being a nondestructive, time-efficient, relatively inexpensive and accurate means of analyzing homogenous materials like obsidian. Briefly, the sample is bombarded with a focused beam of x-rays that has enough energy to ionize atoms in the sample (i.e., it expels electrons from the inner orbitals of the atoms). Electrons in the outer orbitals move to fill the empty holes in the inner orbitals and, in doing so, release energy in amounts that are characteristic of both the element and the

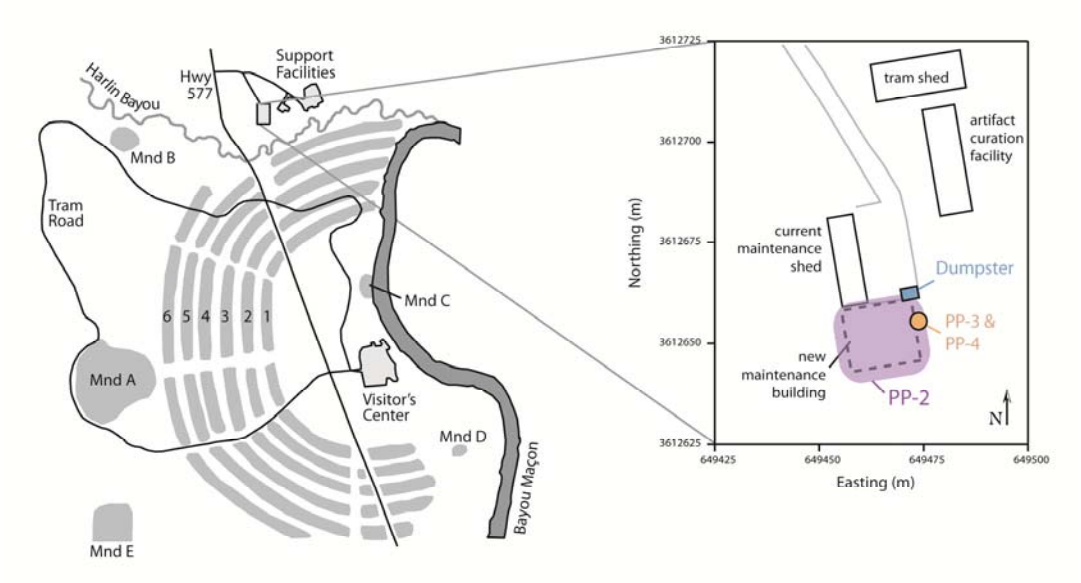

Figure 4. Location of obsidian fragments PP-2, PP-3 and PP-4.

orbital transition (the energy difference between the original outer and the final inner orbitals). Spectrometers measure the amount of released energy; from this, the elements present and their concentrations can be calculated.

The four archaeological obsidian fragments and a sample of obsidian used recently by park knappers were analyzed on an energy dispersive XRF spectrometer following a well-established protocol (e.g., Hughes 1988, 1994). The x-ray tube was operated at differing voltages and current settings to optimize excitation of rubidium (Rb), strontium (Sr), yttrium (Y), zirconium (Zr) and niobium (Nb); barium (Ba), titanium (Ti), iron (Fe), and manganese (Mn) were analyzed as well. X-ray tube current was scaled to the physical size of each specimen. Following the acquisition of x-ray spectra and the extraction of elemental intensities, matrix correction algorithms were used to compensate for absorption and enhancement effects. Then, the elemental peak intensities for each specimen were converted to concentrations (parts per million or weight %) using calibrations derived from up to 30 rock standards. Whereas quantitative analysis is based on elemental concentrations, semi-quantitative analysis relies on the elemental intensity ratios of Rb/Sr/Zr, Fe/Mn, and Zr/Nb (Hughes 2007, 2010). For both quantitative and semi-quantitative analyses, the goal is to determine if the elemental compositions of the archaeological unknowns fall within 2 standard deviations of the mean of known obsidian chemical group "sources" (*sensu* Hughes 1998).

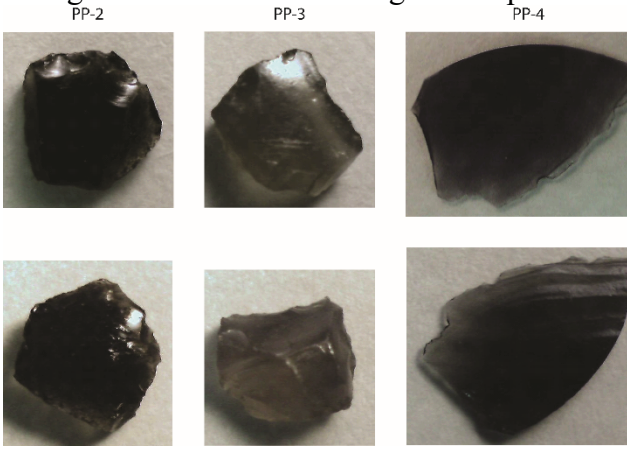

Figure 5. Obsidian fragments PP-2, PP-3 and PP-4, recovered in 2009.

	PP-1	Knapper's Sample	Standard RGM-1
Ba (Barium)	1238 ± 32	1321 ± 32	805 ± 28
$Fe_2O_3^T$ (Iron Oxide) wt. %	1.53 ± .02	.98 ± .02	1.87 ± .02
Fe/Mn (Iron/Manganese ratio)	39	27	61
Mn (Manganese)	410 ± 8	-	283 ± 8
Nb (Niobium)	7 ± 3	9 ± 3	11 ± 3
Rb (Rubidium)	81 ± 4	99 ± 4	149 ± 4
Sr (Strontium)	104 ± 3	70 ± 3	111 ± 3
Ti (Titanium)	1185 ± 32	-	1622 ± 36
Y (Yttrium)	25 ± 3	25 ± 3	24 ± 3
Zr (Zirconium)	128 ± 4	96 ± 4	221 ± 4

Table 2. Quantitative ED-XRF data for PP-1 and the knapper's sample from Poverty Point. Values in parts per million (ppm) except where indicated. ±2 σ estimate of x-ray counting uncertainty and regression fitting error at 120=240 seconds livetime.

Neutron Activation Analysis

Neutron activation analysis (NAA) is another commonly used method for establishing the geochemical source of obsidian samples. NAA is destructive and more time-consuming and expensive than XRF, but it can analyze smaller samples, measure more elements, and measure certain other elements with greater precision than XRF. Briefly, this method works by bombarding the sample with a controlled flux of neutrons, creating radioactive isotopes of the elements in the sample. As the radioactive isotopes decay, they produce characteristic emissions which are counted and used to identify and quantify the elemental composition of the sample. The University of Missouri Research Reactor (MURR) has the largest database of archaeologically relevant obsidian sources in the world (n ≈ 800) and all four obsidian artifacts were sent to MURR.

A sample of PP-1 was removed; PP-2, PP-3, and PP-4 were used entirely. Following a standard protocol, the samples were split into two subsamples, crushed and placed into vials prior to irradiation (Ambrose et al. 2001; Glascock et al. 1989). One subsample underwent a 5-second irradiation, followed by a 25-minute decay period and 12-minute counting time to obtain concentrations of barium (Ba), chlorine (Cl), dysprosium (Dy), potassium (K), manganese (Mn) and sodium (Na). The other subsample was irradiated for 70 hours, followed by a 7-8 day decay period and 2000-second counting time for barium (Ba), lanthanum (La), lutetium (Lu), neodymium (Nd), samarium (Sm), uranium (U) and ytterbium (Yb) concentrations; after 4-5 weeks of further decay, they were counted again for 10,000 seconds to determine cerium (Ce), cobalt (Co), cesium (Cs), europium (Eu), iron (Fe), hafnium (Hf), rubidium (Rb), antimony (Sb), scandium (Sc), strontium (Sr), tantalum (Ta), terbium (Tb), thorium (Th), zinc (Zn) and zirconium (Zr) concentrations.

Figure 6. Poverty Point's obsidian, PP-1 through PP-4.

Obsidian Hydration Analysis

Because the obsidian fragments came from surface and near surface contexts at Poverty Point, their association with the Late Archaic occupation of the site is far from certain. Fortunately, obsidian hydration analysis can be used to assess the relative age of the artifacts. This method relies on the observation that when the surface of obsidian is exposed to the atmosphere, the material begins to absorb water, creating a band of increased density

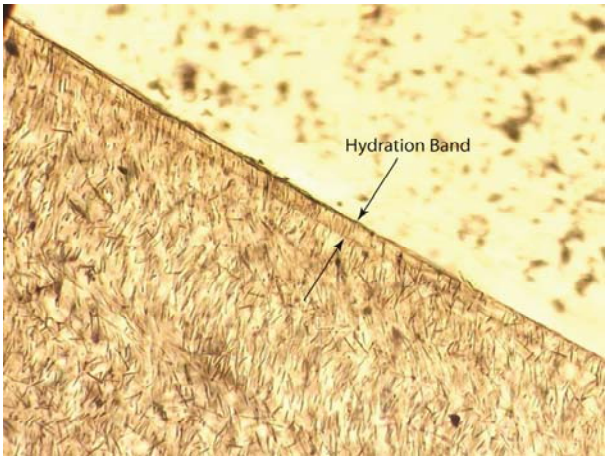

Figure 7. Well-developed hydration band along specimen edge.

known as a hydration band (Friedman and Smith 1960). The band's thickness depends on factors like time since exposure, ambient temperature, and the composition of the obsidian.

A freshly exposed surface will not have a hydration band and it may take as long as 70 years for a band to enlarge sufficiently so that it is readily detectable. A well-developed hydration band is relatively easy to see and measure (Figure 7). Selection of the surface for analysis is critical as remnant surfaces produced by geological processes prior to human alteration will give erroneously old ages, while more recently exposed (e.g., prehistoric scavenging and recycling of older items) and newly exposed (e.g., damaged during excavation, processing or curation) surfaces will give erroneously young ages. Surficial weathering is another complicating factor; pitting and erosion due to wind (sand blasting), fire or trampling can reduce the thickness of the hydration band, thereby leading to underestimates of an artifact's age. Some forms of weathering also can destroy the hydration band's diffusion front, making it indistinct and creating what is known as diffuse hydration. Figure 8 illustrates good examples of surficial pitting from weathering and an indistinct diffusion front (i.e., diffuse hydration).

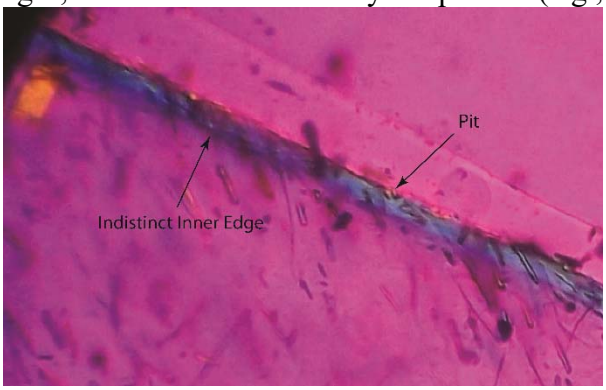

Figure 8. Enhanced image showing an indistinct (diffuse) hydration front on the inner edge and pitting due to weathering on the outer edge.

A small slice (approximately 1 mm thickness) of material that transected at least two surfaces was removed from each fragment. The slices were mounted on etched glass micro-slides, ground to translucency and examined microscopically for the presence of hydration bands. Error in measuring hydration band thickness is ± .2 µm. Although no region-specific calibration curves, which would allow estimation of the age of obsidian artifacts, have been established for the Lower Mississippi Valley, artifacts associated with recent knappers should be distinguishable from those associated with the Poverty Point occupation. A recently exposed surface will have no hydration band, whereas a 3,500 year old surface may have a hydration band 4-5 µm thick.

Results and Discussion

X-Ray Fluorescence

Only PP-1 and the knapper's sample were large enough to produce quantitatively reliable results with XRF (Table 2). The maintenance building fragments (PP-2, PP-3 and PP-4) were analyzed semi-quantitatively and those results are presented in Table 3, along with PP-1 for comparison. Reanalysis of the Gibson sample, PP-1, affirmed the earlier conclusion that the specimen does not match any archaeologically-

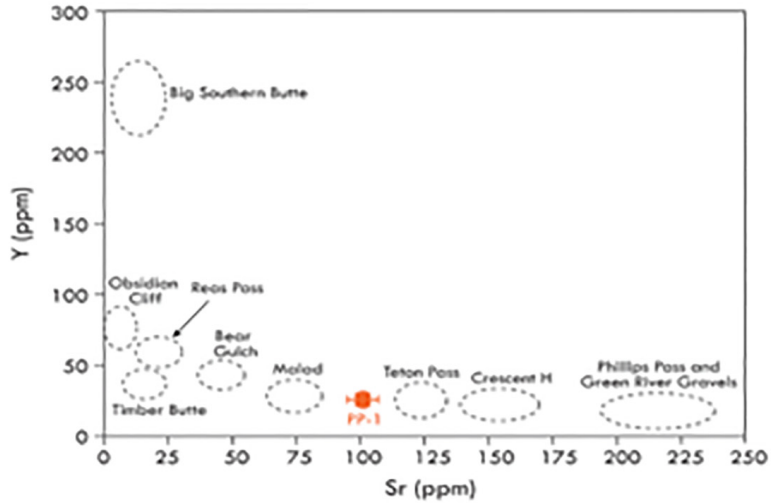

Figure 9. PP-1 versus archaeologically significant North American obsidian source samples.

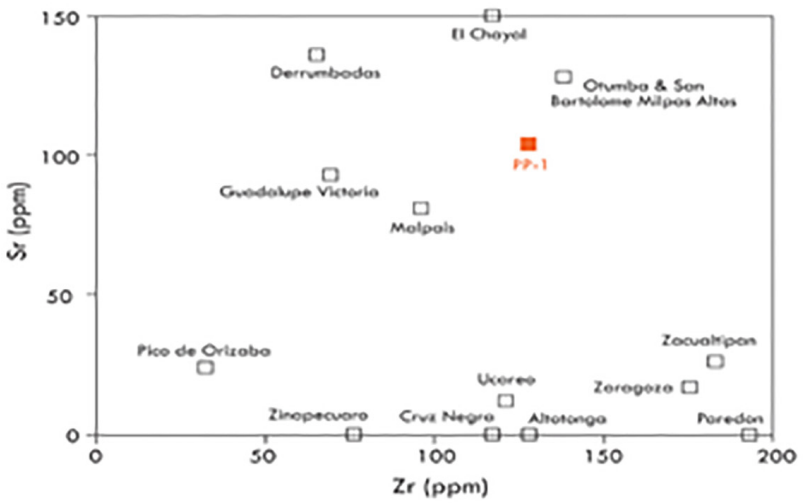

Figure 10. PP-1 versus archaeologically significant Mexican and Mesoamerican obsidian source samples.

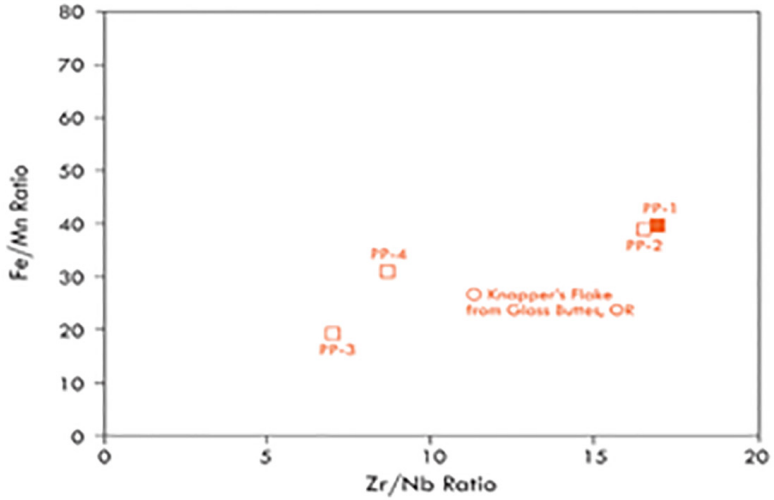

Figure 11. Semi-quantitative Fe/Mn vs. Zr/Nb intensity ratios for the Poverty Point obsidian fragments and the knapper's sample from the Glass Buttes Complex, Oregon.

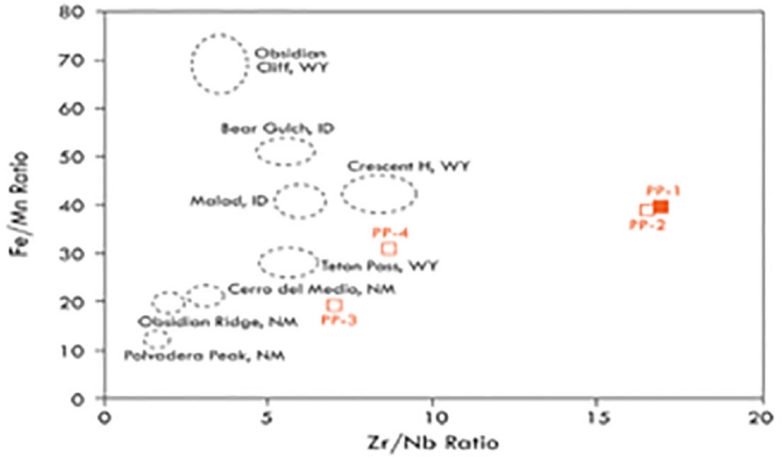

Figure 12. Semi-quantitative Fe/Mn vs. Zr/Nb intensity ratios for t he Poverty Point obsidian fragments and archaeologically significant western North American obsidian source samples.

significant geological obsidian sources from the western United States within the database at the Geochemical Research Laboratory (Figure 9). Nor, does it match the trace element composition of archaeologically-significant geological obsidians from Mesoamerica or Mexico (Figure 10). Figure 10 plots PP-1 with a subset of Mexican and Mesoamerican obsidian that falls within the general range of its composition, but there is no close match.

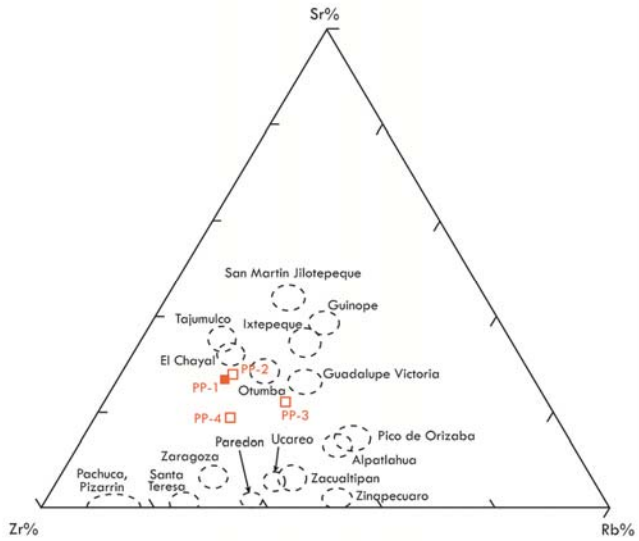

Figure 13. Semi-quantitative rubidium, strontium, and zirconium concentrations for Poverty Point obsidian.

Close correspondence in trace element intensity ratios between PP-1 and PP-2, the first maintenance building fragment found, indicates those two are most likely from the same, unknown, geochemical source (Figure 11). PP-3 and PP-4, on the other hand, appear to be geochemically distinct from PP-1/PP-2, and from each other. Thus, the XRF data indicate three different geochemical sources represented in the four obsidian fragments from Poverty Point. The elemental composition of the recent knapper's sample is consistent with the Glass Buttes source attribution and is not geochemically similar to any of the archaeological fragments. The Poverty Point State Historic Site, however, has hosted many flintknappers over the past 30 years or so, and they probably did not restrict their obsidian to the Glass Buttes Complex.

Much as specimen PP-1 is quantitatively distinct from the significant western North American obsidians, they all are semi-quantitatively distinct from those sources in terms of their Fe/Mn vs. Zr/Nb compositions (Figure 12). Equally important, none of the Poverty Point specimens match the trace element signature of obsidian artifacts identified in archaeological sites of the Great Plains, Rocky Mountains, American Southwest, or Midwestern United States. None of the four specimens match the Rb/Sr/Zr profiles of geological obsidians from Mexico or Mesoamerica, either (Figure 13). The PP-1/PP-2 fragments are somewhat similar in terms of their Rb/Sr/Zr composition to the El Chayal obsidian of Guatemala; but they are not even close to El Chayal or other Mesoamerican obsidian sources when other elements are plotted (Figure 14). Although this analysis could not establish where Poverty Point's obsidian samples came from, it did rule out many possible geological sources, including those known in Wyoming.

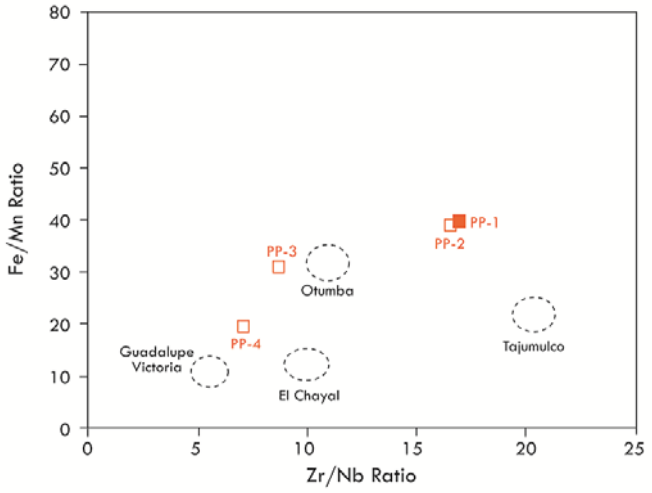

Figure 14. Semi-quantitative Fe/Mn vs. Zr/Nb intensity ratios for the Poverty Point obsidian fragments and a subsample of archaeologically significant Mesoamerican geological source samples.

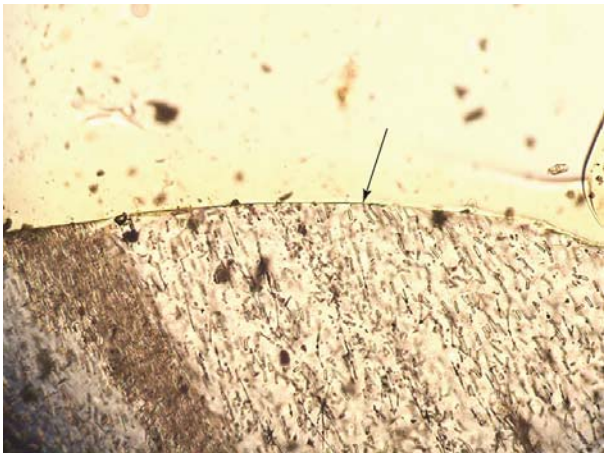

Figure 15. Poverty Point obsidian thin-section showing lack of a hydration band at its surface.

Obsidian Hydration Analysis

When the XRF analyses failed to find a geochemical match for the Poverty Point obsidian fragments, this increased the likelihood that the obsidian fragments were not prehistoric in origin. Obsidian hydration analysis was the only way to establish the relative age of the artifacts. No hydration bands were detected on any of the artifacts' sampled surfaces (Figure 15). The absence of visible bands could be a result of weathering (e.g., damage by fire), but this seems highly unlikely given the apparent lack of weathering elsewhere on the artifacts. It is most likely that the obsidian artifacts are recent in origin as the product of modern flintknappers. The obsidian does not represent a westward extension of the Poverty Point exchange network, but reveals the apparently broader acquisition network of modern flintknappers.

Neutron Activation Analysis

Even though the matter of where the obsidian originated is not relevant to understanding the Late Archaic culture at Poverty Point, it continues to be an intriguing question. Thus, when offered, we took advantage of the opportunity to apply a different method with a larger database of known geochemical sources of obsidian. Table 4 presents the elemental compositions of the four obsidian fragments as measured with NAA.

As with the XRF results, PP-1 and PP-2 were determined via NAA to have come from the same geochemical source. The NAA results, however, produced a match with Glass Buttes A, one of the geochemically distinct subsources of the Glass Buttes Complex in Oregon (Ambrose et al. 2001). Glass Buttes is known to be a common source for obsidian used by modern flintknappers, as evidenced by park knappers' recent use of that source. This is consistent with the conclusion of the obsidian hydration analysis that the fragments are recent in origin.

PP-3 and PP-4 came from geochemical sources distinct from PP-1/PP-2 and distinct from each other. Those sources remain unknown. PP-3 and PP-4 don't even match the geochemical fingerprint of any other archaeological artifacts in the database. We can only surmise that some modern knappers have had access to obsidian sources in areas that haven't been completely characterized (e.g., northern Mexico) or that weren't used prehistorically and that is why they are not in the archaeologically-relevant database.

Conclusions

A single piece of obsidian discovered at Poverty Point 25 years ago was taken as evidence for a westward extension of the prehistoric trade network. Although (or because) a definitive report was lacking, the source attribution remained essentially unchallenged. Indeed, it was the new discovery of three more obsidian fragments that spurred an effort to resolve the status of obsidian as a *bona fide* prehistoric raw material at Poverty Point. Those three new fragments were recovered using ⅛" mesh screens. Had a larger screen size been used, they would not have been recovered and the status of Poverty Point obsidian would likely have remained as it was.

.

	PP-1	PP-2	PP-3	PP-4
Element Intensities:				
Rb (Rubidium)	153	125	163	145
Sr (Strontium)	217	175	117	116
Zr (Zirconium)	438	329	237	336
∑ Rb, Sr, Zr	808	629	517	597
Rb%	.189	.199	.315	.243
Sr%	.269	.278	.226	.194
Zr%	.542	.523	.459	.563
Intensity Ratios:				
Fe/Mn (Iron/Manganese)	40.1	39.2	19.3	31.0
Rb/Sr (Rubidium/Strontium)	.7	.7	1.4	1.3
Sr/Y (Strontium/Yttrium)	3.1	3.4	3.6	1.1
Y/Nb (Yttrium/Niobium)	2.7	2.6	1.0	2.7
Zr/Nb (Zirconium/Niobium)	16.9	16.5	7.0	8.6
Zr/Y (Zirconium/Yttrium)	6.4	6.5	7.2	3.2

Table 3. Semi-quantitative XRF data for all obsidian fragments from Poverty Point. Elemental intensities (net peak counts/second above background) generated at 30 seconds livetime.

XRF analysis showed that Poverty Point's obsidian was not from Wyoming, nor was it linked with any of the well-known, major geological obsidian sources in the western United States, Mexico, or Mesoamerica. In fact, there appear to be three different sources represented in the four fragments. Additional geochemical research, using NAA, affirmed that the four fragments came from three distinct geochemical sources and a more extensive database allowed two fragments to be identified as having come from subsource A of the Glass Buttes Complex in Oregon. The sources of the other two artifacts remain unidentified. The absence of visible hydration bands on any of the specimens provided evidence that the four obsidian artifacts are not prehistoric in origin. Thus, in this case, we conclude that the geochemical sources of these Poverty Point obsidian specimens have no relevance to the Late Archaic culture or its prehistoric trade network.

Acknowledgments

Our thanks go to Jeffrey Ferguson and Michael Glascock of MURR for conducting the analysis by NAA. We would also like to acknowledge Dennis LaBatt, former Poverty Point site manager, for agreeing that determining the source of Poverty Point's obsidian was important enough to merit destructive analysis via NAA. Thank you, too, to Dennis Jones for insisting that the article be included in *Louisiana Archaeology* and for his endless patience and good humor while waiting for it to be prepared.

The research that is the subject of this article was conducted through the State of Louisiana's Poverty Point Station Archaeology Program, based at the University of Louisiana at Monroe. It has been financed with state funds and with federal funds from the National Park Service, U.S. Department of the Interior, through the Department of Culture, Recreation, and Tourism, Office of Cultural Development, Division of Archaeology.

	PP-1	PP-2	PP-3	PP-4
Al (Aluminum)	66013.5	72600.4	71024.3	64703.0
Ba (Barium)	1195.70	1217.50	814.80	1185.20
Br (Bromine)	.000	.000	.000	2.504
Ce (Cerium)	43.7214	44.5411	49.9312	74.5932
Cl (Chorine)	79.0	140.4	297.5	160.4
Co (Cobalt)	1.4731	1.4251	.1924	.4135
Cs (Cesium)	2.9329	3.0445	1.4707	4.3672
Dy (Dysprosium)	3.5628	3.8794	2.5961	6.8554
Eu (Europium)	.7409	.7506	.6277	.7026
Fe (Iron)	10813.1	10460.5	4144.2	9037.2
Hf (Hafnium)	4.5100	4.4400	2.7900	6.0200
K (Potassium)	34906.4	32378.5	39728.4	30215.4
La (Lanthanum)	22.9500	23.4600	24.6200	42.1500
Lu (Lutetium)	.4600	.3700	.4900	.6200
Mn (Manganese)	375.89	364.92	455.35	305.63
Na (Sodium)	28417.9	28677.8	29077.3	32132.8
Nd (Neodymium)	20.1700	19.5200	21.8000	30.3800
Rb (Rubidium)	85.00	85.98	41.18	171.63
Sb (Antimony)	.2900	.2200	.2200	.5100
Sc (Scandium)	3.9900	3.7400	2.1800	3.0600
Sm (Samarium)	3.6100	3.4900	4.2600	4.8100
Sr (Strontium)	130.41	137.77	0.00	149.95
Ta (Tantalum)	.6000	.6000	.4700	1.6300
Tb (Terbium)	.5600	.5400	.6500	.5900
Th (Thorium)	7.3900	7.6000	4.9900	15.8500
U (Uranium)	3.0600	3.6200	1.2300	6.1500
Yb (Ytterbium)	3.0300	2.6300	3.1400	3.8800
Zn (Zinc)	42.96	34.87	23.48	45.67
Zr (Zirconium)	115.17	209.83	66.88	263.50
Chem Group	GB8-OR	GB8-OR	Unassigned	Unassigned

Table 4. Elemental concentrations for archaeological obsidian fragments from Poverty Point measured by NAA. Elemental concentrations are in parts per million (ppm). Analytical uncertainty for NAA measurement of La, Sm, Yb, Ce, Cs, Eu, Fe, Hf, Rb, Sc, Th, Mn, and Na is ca. 2-3%; uncertainties for Ba, Lu, Co, Sb, Ta, Tb, Zn, Al, Dy, and K range from 3-10%, and uncertainties for Nd, U, Sr, Zr, and Cl range from ca. 10-20% (M. Glascock, personal communication, 2013).

References Cited

Ambrose, J. A., M. D. Glascock, and C. E. Skinner (2001) Chemical Differentiation of Obsidian within the Glass Buttes Complex, Oregon. *Journal of Archaeological Science* 28: 741-746.

Anderson, D., C. Gillam, C. Carr, T. Emerson, and J. Gibson (2007) Resolving Interaction Networks in Eastern North America. Paper presented at the 72nd Annual Meeting of the Society for American Archaeology, Austin, Texas.

Anderson, D. G., and K. E. Sassaman (2009) Recent Developments in Southeastern Archaeology. Paper presented at the 66th Annual Meeting of the Southeastern Archaeological Conference, Mobile, Alabama.

Braly, B. R., and J. L. Sweat (2008) An Analysis of Obsidian and Other Archaeological Materials from the Southeast Portion of Neelys Bend on the Cumberland River, Davidson County, Tennessee. *Tennessee Archaeology* 3: 131-138.

Connolly, R. P. (2006) An Assessment of Radiocarbon Age Results from the Poverty Point Site. *Louisiana Archaeology* 27: 1-14.

Friedman, I., and R. L. Smith (1960) A New Dating Method Using Obsidian: Part 1. The Development of the Method. *American Antiquity* 25: 476-522.

Gibson, J. (1990) Over the Mountain and Across the Sea: Regional Poverty Point Exchange. *Louisiana Archaeology* 17: 251-299.

Gibson, J. (1994) Empirical Characterization of Exchange Systems in Lower Mississippi Valley Prehistory. In *Prehistoric Exchange Systems in North America*, edited by Timothy G. Baugh and Jonathon E. Ericson, pp. 127-175. Plenum Press, New York.

Gibson, J. (1999) Swamp Exchange and the Walled Mart: Poverty Point's Rock Business. *Raw Materials and Exchange in the Mid-South*, *Proceedings of the 16th Annual Mid-South Archaeological Conference*, edited by Evan Peacock and Samuel O. Brookes, pp. 57-63. Mississippi Department of Archives and History, Jackson, Mississippi.

Gibson, J. (2000) *The Ancient Mounds of Poverty Point: Place of Rings*. University Press of Florida, Gainesville, Florida.

Gibson, J. (2010) Poverty Point Redux. In *Archaeology of Louisiana*, edited by Mark A. Rees, pp. 77-96. Louisiana State University Press, Baton Rouge, Louisiana.

Glascock, M. D., G. E. Braswell, and R. H. Cobean (1998) A Systematic Approach to Obsidian Source Characterization. In *Archaeological Obsidian Studies: Method and Theory*, edited by M. Steven Shackley, pp. 15-65. Plenum Press, New York.

Greenlee, D. M. (2009) *2009 Annual Report of the Station Archaeology Program at Poverty Point State Historic Site*. Unpublished report submitted to the Division of Archaeology, Louisiana Department of Culture, Recreation and Tourism, Baton Rouge, Louisiana. Department of Geosciences, University of Louisiana at Monroe, Monroe, Louisiana.

Hammerstedt, S. W., M. D. Glascock, and C. E. Skinner (2010) Obsidian Artifacts from Moundville. *Journal of Alabama Archaeology* 54: 53-60.

Hill, M. A., D. M. Greenlee, and H. Neff (2010) Sourcing Poverty Point Copper: Testing the Lake Superior Hypothesis using LA-ICPMS Analysis. Paper presented at the 75th Anniversary Meeting of the Society for American Archaeology, St. Louis, Missouri.

Hughes, R. E. (1988) The Coso Volcanic Field Reexamined: Implications for Obsidian Sourcing and Hydration Dating Research. *Geoarchaeology* 3: 253-265.

Hughes, R. E. (1994) Intrasource Chemical Variability of Artefact-Quality Obsidians from the Casa Diablo Area, California. *Journal of Archaeological Science* 21: 263-271.

Hughes, R. E. (1998) On Reliability, Validity, and Scale in Obsidian Sourcing Research. In *Unit Issues in Archaeology: Measuring Time, Space, and Material*, edited by Ann F. Ramenofsky and Anastasia Steffen, pp. 103-114. University of Utah Press, Salt Lake City.

Hughes, R. E. (2007) The Geologic Sources for Obsidian Artifacts from Minnesota Archaeological Sites. *The Minnesota Archaeologist* 66: 53-66.

Hughes, R. E. (2010) Determining the Geologic Provenance of Tiny Obsidian Flakes in Archaeology Using Nondestructive EDXRF. *American Laboratory* 42(7): 27-31.

Hughes, R. E., M. Kay, and T. J. Green (2002) Geochemical and Microwear Analysis of an Obsidian Artifact from the Brown Bluff Site (3WA10), Arkansas. *Plains Anthropologist* 47: 73-76.

Jeane, D. (1984) A Possible Paleo-Indian Obsidian Tool from Northwest Louisiana. *Louisiana Archaeological Society Newsletter* 11(2): 5.

Norton, M. R. (2008) Obsidian Research in Tennessee and Alabama. *Tennessee Archaeology* 3: 123-130.

Origer, T. M. (1989) Hydration Analysis of Obsidian Flakes Produced by Ishi During the Historic Period. In *Current Directions in California Obsidian Studies*, edited by Richard E. Hughes, pp. 69-77. Contributions of the University of California Archaeological Research Facility No. 48. Berkeley.

Peacock, E., C. Jenkins, and G. White (2006) Obsidian Artifacts from Mississippi. *Mississippian Archaeology* 41: 33-50.

Skinner, C. E. (2007) X-Ray Fluorescence Analysis of an Artifact Obsidian from the Doug Schultz Site, LaSalle Parish, Louisiana. *Northwest Research Obsidian Studies Laboratory Report* 2007-89.

White, N. M., and R. A. Weinstein (2008) The Mexican Connection and the Far West of the U.S. Southeast. *American Antiquity* 73: 227-277.

*Note: this article was previously published as:

Greenlee, Diana M., Richard E. Hughes and Thomas M. Origer (2014) Poverty Point's Obsidian. *Louisiana Archaeology* 37: 89-107.

ABOUT OUR WEB SITE

The IAOS maintains a website at http://members.peak.org/~obsidian/
The site has some great resources available to the public, and our webmaster, Craig Skinner, continues to update the list of publications and must-have volumes.

You can now become a member online or renew your current IAOS membership using PayPal. Please take advantage of this opportunity to continue your support of the IAOS.

Other items on our website include:

- World obsidian source catalog
- Back issues of the *Bulletin.*
- An obsidian bibliography
- An obsidian laboratory directory
- Photos and maps of some source locations
- Links

Thanks to Craig Skinner for maintaining the website. Please check it out!

CALL FOR ARTICLES

Submissions of articles, short reports, abstracts, or announcements for inclusion in the *Bulletin* are always welcome. We accept electronic media on CD in MS Word. Tables should be submitted as Excel files and images as .jpg files. Please use the *American Antiquity* style guide for formatting references and bibliographies.
http://www.saa.org/Portals/0/SAA/Publications/StyleGuide/StyleGuide_Final_813.pdf

Submissions can also be emailed to the *Bulletin* at IAOS.Editor@gmail.com Please include the phrase "IAOS Bulletin" in the subject line. An acknowledgement email will be sent in reply, so if you do not hear from us, please email again and inquire.

Deadline for Issue #60 is December 1, 2018.

Email or mail submissions to:

Dr. Carolyn Dillian
IAOS Bulletin, Editor
Department of Anthropology & Geography
Coastal Carolina University
P.O. Box 261954
Conway, SC 29528
U.S.A.

Inquiries, suggestions, and comments about the *Bulletin* can be sent to IAOS.Editor@gmail.com
Please send updated address information to Matt Boulanger at Boulanger.Matthew@gmail.com

MEMBERSHIP

The IAOS needs membership to ensure success of the organization. To be included as a member and receive all of the benefits thereof, you may apply for membership in one of the following categories:

Regular Member: $20/year*
Student Member: $10/year or FREE with submission of a paper to the *Bulletin* for publication. Please provide copy of current student identification.
Lifetime Member: $200

Regular Members are individuals or institutions who are interested in obsidian studies, and who wish to support the goals of the IAOS. Regular members will receive any general mailings; announcements of meetings, conferences, and symposia; the *Bulletin*; and papers distributed by the IAOS during the year. Regular members are entitled to vote for officers.

*Membership fees may be reduced and/or waived in cases of financial hardship or difficulty in paying in foreign currency. Please complete the form and return it to the Secretary-Treasurer with a short explanation regarding lack of payment.

NOTE: Because membership fees are very low, the IAOS asks that all payments be made in U.S. Dollars, in international money orders, or checks payable on a bank with a U.S. branch. Otherwise, please use PayPal on our website to pay with a credit card.
http://members.peak.org/~obsidian/

For more information about membership in the IAOS, contact our Secretary-Treasurer:

Matthew Boulanger
Department of Anthropology
Southern Methodist University
P.O. Box 750336
Dallas, TX 75275-0336
U.S.A.
Boulanger.Matthew@gmail.com

Membership inquiries, address changes, or payment questions can also be emailed to Boulanger.Matthew@gmail.com

ABOUT THE IAOS

The International Association for Obsidian Studies (IAOS) was formed in 1989 to provide a forum for obsidian researchers throughout the world. Major interest areas include: obsidian hydration dating, obsidian and materials characterization ("sourcing"), geoarchaeological obsidian studies, obsidian and lithic technology, and the prehistoric procurement and utilization of obsidian. In addition to disseminating information about advances in obsidian research to archaeologists and other interested parties, the IAOS was also established to:

1. Develop standards for analytic procedures and ensure inter-laboratory comparability.
2. Develop standards for recording and reporting obsidian hydration and characterization results
3. Provide technical support in the form of training and workshops for those wanting to develop their expertise in the field.
4. Provide a central source of information regarding the advances in obsidian studies and the analytic capabilities of various laboratories and institutions

MEMBERSHIP RENEWAL FORM

We hope you will continue your membership. Please complete the renewal form below.

NOTE: You can now renew your IAOS membership online! Please go to the IAOS website at http://members.peak.org/~obsidian/ and check it out! Please note that due to changes in the membership calendar, your renewal will be for the next calendar year. Unless you specify, the *Bulletin* will be sent to you as a link to a .pdf available on the IAOS website.

___ Yes, I'd like to renew my membership. A check or money order for the annual membership fee is enclosed (see below).

___ Yes, I'd like to become a new member of the IAOS. A check or money order for the annual membership fee is enclosed (see below). Please send my first issue of the IAOS *Bulletin*.

___ Yes, I'd like to become a student member of the IAOS. I have enclosed either an obsidian-related article for publication in the IAOS *Bulletin* or an abstract of such an article published elsewhere. I have also enclosed a copy of my current student ID. Please send my first issue of the IAOS *Bulletin.*

NAME: _____

TITLE: _____ AFFILIATION:_____

STREET ADDRESS: _____

CITY, STATE, ZIP: _____

COUNTRY: _____

WORK PHONE: _____ FAX: _____

HOME PHONE (OPTIONAL): _____

EMAIL ADDRESS: _____

My check or money order is enclosed for the following amount (please check one):
___ $20 Regular
___ $10 Student (include copy of student ID)
___ FREE Student (include copy of article for the *IAOS Bulletin* and student ID)
___ $200 Lifetime

Please return this form with payment: (or pay online with PayPal http://members.peak.org/~obsidian/)

Matthew Boulanger
Department of Anthropology
Southern Methodist University
P.O. Box 750336
Dallas, TX 75275-0336
U.S.A.